Available online at www.sciencedirect.com
ScienceDirect
Cement and Concrete Research 37 (2007) 1379–1410
Cement and Concrete Research

Thermodynamic properties of Portland cement hydrates in the system $CaO–Al_2O_3–SiO_2–CaSO_4–CaCO_3–H_2O$

Thomas Matschei [a,*], Barbara Lothenbach [b], Fredrik P. Glasser [a]

[a] *Department of Chemistry, University of Aberdeen, Meston Building, Meston Walk, Old Aberdeen, AB24 3UE Scotland, UK*
[b] *Empa, Swiss Federal Laboratories for Materials Testing and Research, Laboratory for Concrete & Construction Chemistry, Ueberlandstrasse 129, CH-8600 Duebendorf, Switzerland*

Received 31 May 2007; accepted 3 June 2007

Abstract

A database is presented for commonly-encountered cement substances including C–S–H, $Ca(OH)_2$, selected AFm, AFt and hydrogarnet compositions as well as solid solutions. The AFm compositions include strätlingite. The data were obtained for the most part from experiment and many of the predicted reactions were confirmed by focussed experiments. The temperature-dependence of the thermodynamic data for the above phases, determined partly from experiment and partly from thermodynamic estimations, are also tabulated in the range 1 °C to 99 °C. Relative to previous databases, sulfate AFm is shown to have a definite range of stability range at 25 °C thus removing long-standing doubts about its stability in normal hydrated cement pastes. Carbonate is shown to interact strongly with stabilisation of AFm across a broad range of temperatures and, at low temperatures, to substitute into AFt. The new database enables the ultimate hydrate mineralogy to be calculated from chemistry: most solid assemblages, the persistence of C–S–H apart, correspond closely to equilibrium. This realisation means that hydrate assemblages can be controlled. The development of a thermodynamic approach also enables a fresh look at how mineralogical changes occur in response to environmentally-conditioned reactions; several papers showing applications are cited.

Keywords: Thermodynamics; Thermodynamic data; AFm; AFt; Hydrogarnet; Ettringite; Stratlingite; Phase relations

1. Introduction

One of the unsolved problems in the application of Portland cement is to quantify the performance lifetimes of concrete constructions. Quantification is important to evaluate the performance of nuclear waste containments and, increasingly, long-lived infrastructure developments, where quantification has failed to keep pace with the expectation of stakeholders.

Although we have a wealth of empirical evidence on the performance of historic concretes, information on their formulation, emplacement and exposure history is often incomplete and, moreover, the nature of cements supplied today will almost certainly have changed since the original construction. Empirical studies and historic examples have however yielded much useful *qualitative* information on the aggressivity of various service environments. Numerous tests and test methods have been used as indicators of durability but they do not yield generic conclusions and their predictive capabilities are limited. As a consequence, designers of long-lived constructions have at present to rely on perceived wisdom, as interpreted by experts and incorporated into codes of practice.

The changing nature of cements is also of concern. Cement producers are under pressure to lower the specific energy requirements of cement production and reduce gaseous emissions. These goals are presently addressed by a combination of methods; partly by optimisation of process technology, including the use of alternative fuels and raw materials (the impacts of which are beyond the scope of this study), and partly by reliance on supplementary cement materials to lessen the need for energy-rich cement. Although the use of supplementary materials is generally regarded as beneficial in terms of strength and durability as, for example, highlighted by developments in

* Corresponding author.
E-mail addresses: t.matschei@abdn.ac.uk (T. Matschei), f.p.glasser@abdn.ac.uk (F.P. Glasser).

0008-8846/$ - see front matter © 2007 Elsevier Ltd. All rights reserved.
doi:10.1016/j.cemconres.2007.06.002

cement and concrete standards, long term performance is not fully understood. Supplementary materials presently in use include industrial by-products such as slag, fly ash, silica fume, etc. as well as natural materials such as ground limestone, natural pozzolanic and semi-synthetic pozzolans such as metakaolin. Each of these materials has a complex but distinctive chemistry, mineralogy and granulometry. Moreover, each type of material ranges in composition and performance. Studies of their behaviour in blended cements under controlled conditions are confined to selected compositions and short term (1–5 years) laboratory measurements, perhaps supplemented by observations on actual constructions, for which conditions may not be well controlled.

The complexity of blended cement systems and the wide-ranging nature of supplementary cementing materials has meant that guesses – sometimes well informed – have to be made at the outset about what aspects of behaviour should be studied. But the number and complexity of the resulting systems are such that results are often confined to measurement of a few of the many parameters affecting performance. Arguably the most serious question arising from the results of empirical testing is how to extend or extrapolate the results to other compositions and formulations, or to conditions other than those measured, or both. At present we cannot address these issues, except qualitatively.

If quantification of performance is to be achieved, a new paradigm is needed and a key to the development of a successful paradigm must be to concentrate on *generic* approaches. Thermodynamics provides a consistent framework for the analysis of complex systems. Given an adequate database to support calculations, its strength lies in its generic nature; user-defined compositions and conditions can be selected for calculation. This realisation is not new although previous attempts to apply thermodynamics have had only limited success owing partly to deficiencies in the database to enable calculations. In this presentation we concentrate on development of the database.

From an industrial point of view it could be argued that thermodynamic approaches to cement durability are too theoretical and the calculations too difficult to perform. However, the latter is no longer true: geochemists, faced by similar problems of treating complex systems, have developed and validated computer codes capable of being implemented on a PC. Many reliable code packages are available in the public domain. Furthermore codes can be coupled to fluid mass transport modelling modules; in this case, thermodynamic datasets supply important *physical* properties, for example, molar volumes of solid and liquid phases including solid solutions.

Thermodynamics is most readily applied to isochemical systems, i.e., to systems having a constant composition, whereas many cement deterioration reactions involve transport of species into or out of the matrix (or both). In computer-based calculations, such processes also enable more complex conditions to be imposed on the system.

We do not argue that the primary output achieved by application of thermodynamic methods necessarily enables the durability and performance of cements and concretes to be quantified. But we argue that, in the search for quantification, a sound understanding of cement paste mineralogy, and of the ability to calculate features and processes arising from the interaction of cement with potentially aggressive agents introduced from the environment, together with additional possibilities for calculating physical functions and the introduction of kinetic variables, constitutes a great step forward. Other necessary links to develop integrated models of cement performance will be anticipated in discussion.

2. Historical development of cement databases of thermodynamic properties

A thermodynamic database will include many substances for which standard compilations already provide adequate data: it is not necessary to start totally afresh. For example, the thermodynamic properties of water and of many aqueous ions and complexes are well known. Database development focussing on cements is therefore mainly concerned with the properties of solids that are abundant in cements but uncommon or absent in nature. Thus a comprehensive database can be compiled by focussing on relatively few substances.

After years of development, Babushkin et al. published the first reasonably comprehensive compilation of thermodynamic data for cement substances. Their book [1] also gives numerous application examples but, as these are pre-computer, the examples selected for calculation tend to be rather simplistic and at first sight, do not afford significant advance over empirical conclusions. However, a serious problem is that referenced data in this compilation have proved difficult if not impossible to trace to source.

Other databases adding to our knowledge of cement substances have been produced subsequently, e.g., by Atkins et al. [2,3], Damidot [4], Reardon [5,6], Lothenbach and Winnefeld [7], by the Lawrence Livermore National Laboratory [8] and by ANDRA, the French National Agency for Radioactive Waste Management [9]. Studies of phase equilibria, cited subsequently in the text, have also added data on the thermodynamic properties of specific substances.

3. Experimental

A focussed programme of data acquisition was undertaken. This involved synthesis, characterisation, analysis and data integration. New data were obtained through synthesis of phase pure substances with subsequent solubility measurements.

3.1. Analytical procedures

Cement hydrates are generally very sensitive to decomposition by carbonation. Therefore many syntheses and solubility experiments must be performed under N_2 atmosphere to minimize access of atmospheric CO_2. The synthesised solids, aged and stored in inert HDPE or PTFE ware, have been vacuum-filtered with Whatman 540 filter paper and washed several times with ultrapure degassed water to remove alkalis, if present. Subsequently the solids were dried over saturated $CaCl_2$ solution at 37% R.H. for 2 weeks.

Mineralogical examination of the dried solid was made by X-ray diffractometry (XRD) using a PANALYTICAL X'PERT PRO

diffractometer with Cu-Kα-radiation; the angular scan was between 5-80° 2θ with a step size of 0.02 and an average count time of 1 s per step. An environmental scanning electron microscope (ESEM), FEI XL 30, equipped with field emission gun was used to image reaction product morphologies of selected hydrates, e.g. of strätlingite. A METTLER-TOLEDO simultaneous thermal analysis apparatus, TGA/SDTA 851, was used for mass changes and thermal analysis. The observed temperature range was between 30–980 °C at a heating rate of 10 °C/min.

Solutions were obtained by filtration of 15 ml aliquots (30 ml for carbon determination) of the excess solution through a 0.22 μm alkali-resistant MF-millipore membrane syringe filter unit. Part of the solution (10 ml) was acidified with 1 ml 0.1 M HCl for cation analysis; the remainder was used to measure pH and determine anions, e.g. sulfate or carbonate. Solutions awaiting analysis were stored briefly in polypropylene (PP) centrifuge tubes.

Aqueous calcium, aluminium and sodium concentrations were determined by AAS using a VARIAN SPECTRAA 10 flame AAS. A nitrous oxide/acetylene flame was used for calcium and aluminium and an air/acetylene flame for sodium. Where appropriate, samples were diluted with 2500 mg K^+/l solution to suppress ionisation prior to analysis. Sulfate was analysed by ion chromatography with a Dionex DX-120 IC. A 4 mm ion exchange analytical column, IONPAC AS 4A, equipped with a guard column, was fitted for sulfate analysis. The analyte was injected into a 25 μl sample loop and the applied pressure set between 1000–1100 psi (67–74 bars). The eluent used was 1.8 mM Na_2CO_3/l.7 mM $NaHCO_3$; eluent conductivity was suppressed by an ASRS ultra self-regenerating suppressor with deionised water (>18 MΩ cm) regenerant. A spectrophotometric method based on the molybdenum blue method was adopted to determine silicon [10]. A CAMSPEC 301 spectrophotometer was used for spectrophotometric measurements. Carbon was analysed using a LABTOC Analyser by PPM. The detection limit for a reliable TIC (total inorganic carbon) measurement using this method is ~1 mg/l; problems arose with accurate analyses due to the low aqueous concentrations encountered approaching the analytical threshold. The pH (in molal activity scale) was calculated from the bulk composition of the chemical system with the aid of the applied thermodynamic software GEMS-PSI. Additionally, pH was measured at room temperature with a glass electrode suitable for high pH, to enable comparison between calculated and measured pH.

3.2. Synthesis of relevant cement hydrates

The synthesis of the relevant cement hydrates required several solid precursors. These were made from analytical grade (AR) reagents. An important precursor is tricalcium aluminate, C_3A ($Ca_3Al_2O_6$). C_3A was prepared from a 3:1 molar ratio of $CaCO_3$ and Al_2O_3. Lime, CaO, was obtained in a previous step by decarbonation of AR grade $CaCO_3$ at 900 °C for ~12 h. Anhydrite, $CaSO_4$, was used as the sulfate source: it was prepared by dehydration of AR gypsum in a muffle furnace at 750 °C for 5 h.

3.2.1. Hydrogarnet

"Hydrogarnet" is usually defined in the cement literature as the silicon-free composition $Ca_3Al_2(OH)_{12}$. However silicon is a main constituent of Portland and blended Portland cements and the existence of solid solution between katoite, $Ca_3Al_2(OH)_{12}$, and grossularite, $Ca_3Al_2Si_3O_{12}$, is well-known both in the laboratory and from natural occurrences. Siliceous hydrogarnet thus impacts significantly on silicon distribution in cements. To enable thermodynamic calculations, two different compositions were synthesized. $Ca_3Al_2(OH)_{12}$ was prepared by mixing previously synthesised C_3A with boiling water and subsequent ageing at 105 °C in pressurised PTFE bottles for 7 days. A siliceous composition was also prepared with the target composition $Ca_3Al_2SiO_4(OH)_8$, starting from stoichiometric amounts of CaO, $Na_2Si_2O_5{\cdot}2H_2O$, $NaAlO_2$ and water. A slurry of $Na_2Si_2O_5{\cdot}2H_2O$ and $NaAlO_2$ was prepared with an appropriate amount of water. In a separate operation, CaO was suspended in boiling ultrapure water and the slurry containing mixed $Na_2Si_2O_5{\cdot}2H_2O$, $NaAlO_2$ added. Subsequently the preparation was aged for 4 weeks with periodic agitation at 105 °C in sealed PTFE bottles until filtration.

A literature review showed that the synthesis and characterisation of siliceous hydrogarnet is more complicated than the silicon-free variant. Jappy, et al. [11] synthesised hydrogrossular solid solutions $Ca_3Al_2(SiO_4)_{3-x}(OH)_{4x}$ and encountered two different hydrogarnet phases in most preparations. A miscibility gap was postulated to exist at low silica substitutions. However in the title study, one synthesis yielded a single hydrogarnet phase. According to subsequent XRD analysis this solid solution had a rather lower silicon content than the target composition, $Ca_3Al_2SiO_4(OH)_8$. Its silicon content was estimated assuming a linear relation of the unit cell lattice parameter between C_3AH_6 (a_0 ~12.58 Å, PDF 24–217) and grossular, $Ca_3Al_2(SiO_4)_3$ (a_0 ~11.85 Å, PDF 39–368). The unit cell size of the synthetic (a_0 = ~12.39 Å) was calculated by refining its XRD-pattern by least squares minimisation on 14 reflections with the software CELREF using silicon, a_0 = 5.4308 Å as an internal standard (see Fig. 1). Accordingly, its formula was corrected to $Ca_3Al_2(SiO_4)_{0.8}(OH)_{8.8}$. The XRD pattern also contained reflections attributed to C–S–H and most of the "missing" silica and part of the alumina are believed to be present as minor C–S–H impurity.

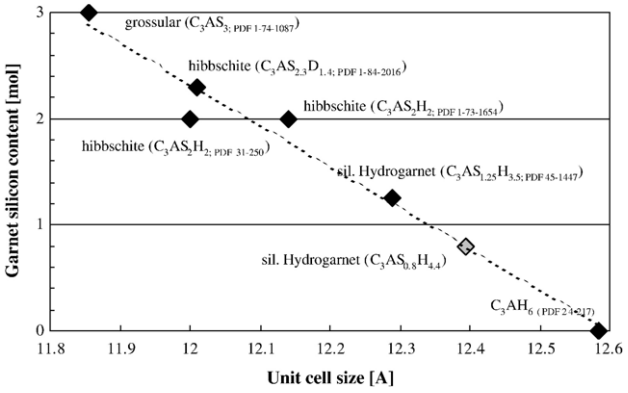

Fig. 1. Estimation of the silicon content of siliceous hydrogarnet; data marked PDF are from the Powder Diffraction File. Data not marked were obtained in the course of the title study (solid compounds). The composition of the synthesised solid solution (open diamond) is estimated by fitting to the curve shown by a dashed line.

3.2.2. AFm phases

Although the stability relations of the AFm phases are known to be sensitive to temperature, few relevant data are available. To enable an estimation of thermodynamic data, the following preparation route yielded suitable material. Since "monosulfoaluminate", $Ca_4Al_2(SO_4)(OH)_{12}\cdot 6H_2O$, becomes more stable at temperatures $>\sim 40$ °C a 1:1 molar mixture of C_3A and $CaSO_4$ was suspended in initially boiling ultra pure water and thereafter kept at 85 °C for 7 days to synthesize phase pure monosulfoaluminate.

"Monocarboaluminate", $Ca_4Al_2(CO_3)(OH)_{12}\cdot 5H_2O$, was prepared by mixing C_3A and $CaCO_3$ in a 1:1 molar ratio with previously degassed ultra pure water at 25 °C and stored with agitation in HDPE-bottles for 14 days until filtration at 25 °C. A second source of monocarboaluminate was prepared by mixing stoichiometric amounts of CaO, $CaCO_3$ and gibbsite ($Al(OH)_3$) with a 0.1 M KOH solution. The suspension was agitated periodically and stored at 50 °C for 4 weeks, with subsequent filtration and washing.

"Hemicarboaluminate", $Ca_4Al_2(CO_3)_{0.5}(OH)_{13}\cdot 5.5H_2O$, was made by addition of C_3A, $CaCO_3$ and CaO in stoichiometric quantities to previously degassed ultra pure water at 25 °C and stored in HDPE-bottles to achieve a successful synthesis. The mixture was aged with stirring for 14 days before filtration.

C_4AH_x, $Ca_4Al_2(OH)_{14}\cdot xH_2O$, was synthesized according to the method of Atkins et al. [12]. C_3A was mixed with CaO in a 1:1 molar ratio at 5 °C using degassed ultrapure water (w/s ~ 10). Afterwards the preparation was stirred for 72 h and periodically agitated, still at 5 °C. After 3 weeks at 5 °C the solid was vacuum filtered under N_2 atmosphere.

Several methods for the preparation of strätlingite, $Ca_2Al_2SiO_2(OH)_{10}\cdot 3H_2O$ are described in the literature (e.g. sol–gel-preparation from glasses, etc). These routes were pursued but the best preparations were obtained by starting from a stoichiometric mix of CaO, $Na_2Si_2O_5\cdot 2H_2O$, $NaAlO_2$ and water at 25 °C. First, all chemicals were separately suspended in ultrapure water at 25 °C. The slurry containing sodium aluminate solution was added to the previously prepared portlandite solution with stirring. Finally the sodium silicate solution was added and the resulting suspension stirred for 4 weeks at 25 °C prior to filtration. HDPE-bottles were used in all stages of the preparation. Unlike other cement hydrates, which are uniformly white, the strätlingite preparation had a pale bluish colour.

3.2.3. AFt phases

The determination of the solubility of SO_4–AFt, ettringite, has been the subject of numerous investigations [12–15]. The literature data show generally good agreement and we therefore concentrated on its less well characterised carbonate analogue, CO_3–AFt or "tricarboaluminate", $Ca_6Al_2(CO_3)_3(OH)_{12}\cdot 26H_2O$, prepared using a modification of the method of Carlson and Berman [16] by precipitation from a stoichiometric mixture of CaO, $NaAlO_2$ and Na_2CO_3 in a 10% w/v sucrose solution. The previously-prepared slurries of sodium aluminate and sodium carbonate were added to the sucrose-portlandite mixture, stirred for 3 days and periodically agitated at 25 °C until filtration after ~ 2 weeks.

3.3. Solubility determinations

Solubility determinations were made at various temperatures between 5° and 105 °C. Two series of reaction mixtures were prepared to derive solubility data for katoite, $Ca_3Al_2(OH)_{12}$. In the experiment from undersaturation, previously synthesized dry $Ca_3Al_2(OH)_{12}$ powder was redispersed in water (water/solid-ratio ~ 30) at 25 °C and then stored in HDPE bottles (at temperatures <70 °C) or PTFE bottles (at temperatures ≥ 70 °C) isothermally at well-spaced intervals between 5°–105 °C prior to analysis. In a second series, a slurry of $Ca_3Al_2(OH)_{12}$, prepared from C_3A as described and aged at 105 °C, was divided into several samples with the aid of a syringe. The sample bottles (HDPE or PTFE) were then filled with boiled water, sealed under N_2 atmosphere and slowly cooled to the desired temperature and held for ~ 4 weeks prior to analysis. The water/solid mass ratio of the second set of samples was deliberately set at ~ 1000 to enable direct comparison with the results of Wells et al. [17], which were also obtained at w/s ~ 1000.

Experiments were conducted from both super- and undersaturation for monosulfoaluminate, for monocarboaluminate made by two different preparative routes, and for hemicarboaluminate at temperatures between 5° and 110 °C. Stoichiometric mixtures of C_3A with either $CaSO_4$ or CaO and $CaCO_3$ (see paragraph 3.2.2) were used at various temperatures in experiments from supersaturation (water/solid-ratio ~ 30). Solubilities from undersaturation were determined by redispersing previously synthesized and characterised single phase solids in ultra pure degassed water (water/solid ratio ~ 30). The samples were analysed after 4–6 weeks reaction time in both cases. Additionally a second dataset for hemicarboaluminate at 25 °C was generated by reaction of monocarboaluminate with synthetic C_4AH_{13} (previously prepared from a 1:1 molar mixture of C_3A and CaO at 5 °C) at a 1:1 molar ratio (water/solid-ratio ~ 30): complete reaction at 5 °C required ~ 3 weeks.

The synthesis of siliceous hydrogarnet, strätlingite and the second source of monocarboaluminate required the addition of sodium and synthesis was thus achieved at high aqueous pH. Most of the sodium could be removed by flushing the filtrates several times with ultra pure degassed water prior to drying. We comment subsequently on the residual sodium contents. Solubilities determined from undersaturation were obtained by redispersing powders of each mineral in ultra pure, degassed water (water/solid ratio ~ 30) and undertaking analyses at well-spaced time intervals.

4. Methods used to derive and manipulate thermodynamic data

4.1. Software and standard databases

Chemical thermodynamic modelling consists of calculating the chemical speciation (i.e. amounts or concentrations of chemical components in all phases present in equilibrium state) from total bulk composition of the system and thermodynamic data for components. In the GEM (Gibbs free energy

Table 1
Standard (partial molal) thermodynamic properties of aqueous species at 25 °C, 1 bar used in GEM calculations

Species	ΔG^{01}	ΔH^0	S^0	C_p^0	V^0	a_1^4	a_2^4	a_3^4	a_4^4	c_1^4	c_2^4	w^4	Ref[5]
	[kJ/mol]	[kJ/mol]	[J/K mol]	[J/K mol]	[cm^3/mol]	[cal/(bar mol)]	[cal/mol]	[calK/(bar mol)]	[calK/mol]	[cal/Kmol]	[calK/mol]	[cal/mol]	
Al^{3+}	−483.71[2]	−530.63	−325.10	−128.70	−45.24	−0.33802	−1700.71	14.5185	−20,758	10.7	−80,600	275,300	[21]
AlO^+ (+H_2O=$Al(OH)_2^+$)	−660.42	−713.64	−112.97	−125.11	0.31	0.21705	−248.11	6.7241	−26,763	−2.5983	−91,455	95,700	[21]
AlO_2^- (+2H_2O=$Al(OH)_4^-$)	−827.48	−925.57	−30.21	−49.04	9.47	0.37221	399.54	−1.5879	−29,441	15.2391	−54,585	174,180	[21]
AlO_2H (aq) (+2H_2O=$Al(OH)_3$ (aq)	−864.28	−947.13	20.92	−209.21	13.01	0.35338	84.85	5.4132	−28,140	−23.4129	−132,195	−3000	[21]
$AlOH^{2+}$	−692.60	−767.27	−184.93	55.97	−2.73	0.20469	−278.13	6.8376	−26,639	29.7923	−3457	172,470	[21]
$AlSO_4^+$	−1250.43	−1422.67	−172.38	−204.01	−6.02	0.13869	−439.2	7.4693	−25,974	−11.6742	−129,914	117,290	[22]
$Al(SO_4)_2^-$	−2006.30	−2338.40	−135.50	−268.37	31.11	0.68275	889.25	2.2479	−31,466	−12.022	−161,447	211,990	[22]
Ca^{2+}	−552.79[2]	−543.07	−56.48	−30.92	−18.44	−0.01947	−725.2	5.2966	−24,792	9	−25,220	123,660	[21]
$CaOH^+$	−717.02	−751.65	28.03	6.05	5.76	0.27243	−113.03	6.1958	−27,322	11.1286	−27,493	44,960	[21]
$CaCO_3$ (aq)	−1099.18	−1201.92	10.46	−123.86	−15.65	−0.03907	−873.25	9.1753	−24,179	−11.5309	−90,641	−3800	[22]
$CaHCO_3^+$	−1146.04	−1231.94	66.94	233.70	13.33	0.3706	126.7	5.252	−28,310	41.722	83,360	30,800	[20]
$CaSO_4$ (aq)	−1310.38	−1448.43	20.92	−104.60	4.70	0.24079	−189.92	6.4895	−27,004	−8.4942	−81,271	−100	[22]
$CaHSiO_3^+$ (+H_2O=$CaSiO(OH)_3^+$)	−1574.24	−1686.48	−8.33	137.80	−6.74	0.10647	−517.87	7.7785	−25,649	30.8048	36,619	58,310	[22]
Na^+	−261.88[2]	−240.28	58.41	38.12	−1.21	0.1839	−228.5	3.256	−27,260	18.18	−29,810	33,060	[21]
NaOH (aq)	−418.12	−470.14	44.77	−13.40	3.51	0.22338	−232.87	6.6683	−26,826	4.0146	−36,863	−3000	[21]
$NaCO_3^-$	−797.11	−938.56	−44.31	−51.28	−0.42	0.23862	−195.21	6.5103	−26,982	15.3395	−55,686	178,700	[23][6]
$NaHCO_3$ (aq)	−847.39	−929.50	154.72	200.33	32.32	0.6173	729.43	2.876	−30,805	33.879	67,193	−3800	[23][6]
$NaSO_4^-$	−1010.34	−1146.66	101.76	−30.09	18.64	0.47945	392.84	4.199	−29,414	13.4899	−45,256	126,060	[23][6]
CO_2 (aq)	−386.02	−413.84	117.57	243.08	32.81	0.62466	747.11	2.8136	−30,879	40.0325	88,004	−2000	[21]
CO_3^{2-}	−527.98	−675.31	−50.00	−289.33	−6.06	0.28524	−398.44	6.4142	−26,143	−3.3206	−171,917	339,140	[21]
HCO_3^-	−586.94[2]	−690.01	98.45	−34.85	24.21	0.75621	115.05	1.2346	−28,266	12.9395	−47,579	127,330	[21]
SO_4^{2-}	−744.46[2]	−909.70	18.83	−266.09	12.92	0.83014	−198.46	−6.2122	−26,970	1.64	−179,980	314,630	[21]
HSO_4^-	−755.81	−889.23	125.52	22.68	34.84	0.69788	925.9	2.1108	−31,618	20.0961	−19,550	117,480	[21]
OH^-	−157.27	−230.01	−10.71	−136.34	−4.71	0.12527	7.38	1.8423	−27,821	4.15	−103,460	172,460	[21]
$HSiO_3^-$ (+H_2O=$H_3SiO_4^-$)	−1014.60	−1144.68	20.92	−87.20	4.53	0.29735	−51.81	5.9467	−27,575	8.1489	−73,123	155,110	[22]
Silica species (temperature correction using $C_p(T)$ integration)						a_0 [J/(mol K)]	a_1 [J/(mol K^2)]	a_2 [J K/mol]	(C_p^0=a_0+a_1T+a_2T^{-2})				
SiO_2 (aq) (+2H_2O=H_4SiO_4 (aq))	−833.41[7]	−887.86	41.34[3]	44.47[3]	16.06	46.94[3]	0.034[3]	−1.13E+06[3]					
Silica species (estimated temperature correction by one and two term temperature extrapolation)[8]						A_0[−]	A_1[−]	A_2[−]	(Log$K$=A_0+A_1T+A_2T^{-1})				
$AlSiO_4^-$ (+3H_2O=$Al(OH)_6SiO^-$)	−1681.44	−1833.98	11.13	−4.58	25.53	0	0	1073.34					
$AlHSiO_3^{2+}$ (+H_2O=$AlSiO(OH)_3^{2+}$)	−1540.55	−1717.55	−304.18	−215.90	−40.72	0	0	2206.31					
$CaSiO_3$ (aq) (+H_2O=$CaSiO_2(OH)_2$ (aq))	−1517.56	−1668.06	−136.68	88.90	15.69	0	0	1371.49					
SiO_3^{2-} (+H_2O=$H_2SiO_4^{2-}$)	−938.51	−1098.74	−80.20	119.83	34.13	−10.0006	0	−3917.5					

[1]Recalculated by Thoenen et al. [23] based on log_k values given in Hummel et al. [19] if not stated otherwise [2]taken from Shock et al. [21] [3]Cp parameters calculated using reference reaction SiO_2 (aq)=SiO_2(amorph) see Table 2 [4]parameters to solve the HKF-equation of state; given in original calorimetric units (see [20–22]) as used in GEM [5]references for HKF parameters and S^0 (see [23] for additional information) [6]HKF parameters predicted using program PRONSPREP [22] [7]taken from slop98.dat (see [20]) [8]AlO_2^- + SiO_2(aq)→$AlSiO_4^-$ (Δ_rS^0=$\Delta_rC_p^0$=0); Al^{3+}+$HSiO_3^-$→$AlHSiO_3^{2+}$ (Δ_rS^0=$\Delta_rC_p^0$=0); SiO_2(aq)+H_2O→SiO_3^{2-}+2H^+ ($\Delta_rC_p^0$=0; Δ_rH^0 taken from [19]); SiO_3^{2-}+Ca^{2+}→$CaSiO_3$ (aq) (Δ_rS^0=$\Delta_rC_p^0$=0).

minimisation) method and GEMS-PSI code [18], the total Gibbs energy of the system is minimised at given temperature and pressure; accordingly, for each component, the standard molar Gibbs energy at the temperature of interest must be provided. Calculations require a database of thermodynamic properties of components (substances), a correct statement of the problem, and a solver of chemical equilibria. In this work we used GEMS-PSI [18] — a software package including a GEM solver, a built-in thermodynamic database [19] and a graphical user interface for easy extension of thermodynamic database to user-defined "projects". This was convenient because not all cement minerals are included in standard databases such as Nagra-PSI [19] supplied within GEMS-PSI package. This database was initially designed in "logK format" for application to codes such as PHREEQC that use law of mass action algorithms at standard conditions (1 bar and 25 °C); to include it in GEMS, the logK values were converted into standard molar Gibbs energies and merged with slop98.dat database [20], which was originally developed for the SUPCRT92 code [20]. For aqueous species, this dataset is based on the HKF (Helgeson–Kirkham–Flowers) equation of state which is used to calculate temperature and pressure corrections up to 1000 °C and 5 kbar; the necessary parameters for aqueous species relevant for cementitious systems are given in [21,22] and are summarised in Table 1. The heat capacity coefficients needed for temperature corrections for most of the minerals in the GEMS databases are also given in the slop98.dat dataset. The database, included in the current software package, GEMS version 2.1, is documented in [23] and is in the public domain [19,20]. Raw data for minerals obtained in the title study have been converted into standard molar thermodynamic properties and added to GEMS-PSI database in order to perform modelling calculations. Temperature corrections for thermodynamic properties of condensed substances (e.g. minerals) used in GEMS are based on the well known standard integration of the heat capacity function (e.g. [24]).

Table 2
Standard molar thermodynamic properties of cement hydrates at 25 °C, 1 bar

Phase	log K_{S0}	$\Delta_f G^0$ [kJ/mol]	$\Delta_f H^0$ [kJ/mol]	S^0 [J/(K mol)]	a_0 [J/(mol K)]	a_1 [J/(mol K^2)]	a_2 [J K/mol]	a_3 [J/(mol $K^{0.5}$)]	$V^{o,II}$ [cm^3/mol]	Ref
Hydrogarnet										
C_3AH_6	−20.84	−5010.1	−5540	419	292[I]	0.561[I]	0	0	150	t.s.
$C_3AS_{0.8}H_{4.4}$	−29.87	−5368.0	−5855	369	109	0.631	−1.95e+06	2560	143	t.s.
AFt										
C_6AsH_{32}	−44.9	−15205.9	−17535	1900	1939[I]	0.789[I]	0	0	707	[77]
C_6AcH_{32}	−46.50	−14565.6	−16792	1858	2042	0.559	−7.78e+06	0	650	t.s.
AFm										
C_4AsH_{12}	−29.26	−7778.5	−8750	821	594[I]	1.168[I]	0	0	309	t.s.
C_4AcH_{11}	−31.47	−7337.5	−8250	657	618	0.982	−2.59e+06	0	262	t.s.
$C_4Ac_{0.5}H_{12}$	−29.13	−7336.0	−8270	713	664	1.014	−1.30e+06	−800	285	t.s.
C_4AH_{13}	−25.40	−7326.6	−8302	700	711	1.047	0	−1600	274	t.s.
C_2AH_8	−13.56	−4812.8	−5433	440	392	0.714	0	−800	184	t.s.
C_2ASH_8	−19.70	−5705.1	−6360	546	438	0.749	−1.13e+06	−800	216	t.s.
C–S–H										
Jennite-type ($C_{1.67}SH_{2.1}$)	−13.17	−2480.8	−2723	140	210	0.120	−3.07e+06	0	78[III]	[77]
Tobermorite-type ($C_{0.83}SH_{1.3}$)	−8.0	−1744.4	−1916	80	85	0.160	0	0	59[III]	[77]
Supplementary data										
Water (H_2O)		−237.2	−286	70	75	0	0	0	18	[20,23]
CAH_{10}	−7.50	−4622.4	−5320	501	151	1.113	0	3200	194	t.s.
SiO_2 (amorph)		−848.9	−903	41	47	0.034	−1.13e+06	0	29[IV]	[30]
Gypsum ($CaSO_4{\cdot}2H_2O$)		−1797.8	−2023	194	91	0.318	0	0	75[IV]	[19,23]
Anhydrite ($CaSO_4$)		−1322.1	−1435	107	70	0.099	0	0	46[IV]	[19,23]
Portlandite ($Ca(OH)_2$		−897.0	−985	83	187	−0.022	0	−1600	33[IV]	[19,23]
Lime (CaO)		−604.0	−635	39	49	0.004	−6.53e+05	0	17[IV]	[19,23]
Calcite ($CaCO_3$)		−1129.2	−1207	93	105	0.022	−2.59e+06	0	37[IV]	[19,23]
Gibbsite ($Al(OH)_3$)		−1151.0	−1289	70	36	0.191	0	0	32[IV]	[19,23]
Clinker phases										
C_3S		−2784.3	−2931	169	209	0.036	−4.25e+06	0	73	[1]
β-C_2S		−2193.2	−2308	128	152	0.037	−3.03e+06	0	52	[1]
C_3A		−3382.3	−3561	205	261	0.019	−5.06e+06	0	89	[1]
C_4AF		−4786.5	−5080	326	374	0.073	0	0	130	[1]

t.s — data obtained in title study [I]see Ederova et al. [27] [II]calculated from unit cell parameters given in Taylor [70] if not stated otherwise [III]see Lothenbach et al. [77][IV] and all aqueous species — see GEMS Nagra-PSI dataset [19,23].

4.2. Estimation of heat capacity

The heat capacity function for solids (at constant pressure) was calculated according to Eq. (1) where a_0, a_1, a_2 and a_3 are empirically derived, temperature independent parameters characteristic of each solid.

$$Cp_T^o = a_0 + a_1 T + a_2 T^{-2} + a_3 T^{-0.5} \quad (1)$$

The heat capacities can be measured experimentally or, as was done here, estimated by using a reference reaction with a solid having a known heat capacity and similar structure. As shown by Helgeson et al. [25], this principle was successfully applied to estimate the heat capacity of silicate minerals by formulating a reaction involving a structurally-related mineral of known heat capacity. Gu et al. [26] used a similar approach to predict equilibrium constants for reactions related to aqueous species. Nevertheless, Helgeson et al. [25] pointed out that this method has limitations due to the differing thermodynamic properties of "water", variously bound loosely as hydrate water or structurally, as OH-groups. To minimise errors associated with the varying strengths of bonding for "water", care was taken to formulate reference reactions so as not to involve "free" water as a substituent in reactions unless appropriate to do so. Table 2 shows the coefficients to determine the heat capacity of reference solids to estimate heat capacity data of the relevant cement hydrates.

The coefficients of the heat capacity function (1) of the relevant cement hydrates were calculated according to reference reactions given in Table 3. Experimentally determined heat capacities by Ederova and Satava [27] and data from the built-in GEMS database [19,23] were used as the basis for the estimation of the unknown coefficients (see Table 2). Analogue structures were used in the calculations, e.g. for "unknown" AFm-phases we used monosulfoaluminate as the model. Assuming the reference reaction Eq. (2), Eq. (3) shows the principle way of calculating the necessary coefficient, $a_{n,A,}$ for component A with the aid of the known coefficients $a_{n,B}$ and $a_{n,C}$ with y moles of component B and z moles of component C.

$$A \rightarrow yB + zC \quad (2)$$

$$a_{n,A} = y \cdot a_{n,B} + z \cdot a_{n,C} \quad (3)$$

Table 2 summarises the resulting coefficients and estimated standard molar heat capacities at 25 °C and 1 bar pressure calculated from Eq. (1).

Table 3
Reference reactions used to estimate heat capacities of cement minerals

Phase	Formula and reference reaction
Siliceous hydrogarnet	$Ca_3Al_2(SiO_4)_{0.8}(OH)_{8.8} + 1.6\ Ca(OH)_2 \rightarrow Ca_3Al_2(OH)_{12} + 0.8SiO_2 + 1.6CaO$
Monocarboaluminate	$Ca_4Al_2(CO_3)(OH)_{12}\cdot 5H_2O + 0.5CaSO_4\cdot 2H_2O + 0.5CaSO_4 \rightarrow Ca_4Al_2(SO_4)(OH)_{12}\cdot 6H_2O + CaCO_3$
Hemicarbolauminate	$Ca_4Al_2(CO_3)_{0.5}(OH)_{13}\cdot 5.5H_2O + 0.25CaSO_4\cdot 2H_2O + 0.75CaSO_4 \rightarrow Ca_4Al_2(SO_4)(OH)_{12}\cdot 6H_2O + 0.5CaCO_3 + 0.5\ Ca(OH)_2$
Hydroxy–AFm	$Ca_4Al_2(OH)_{14}\cdot 6H_2O + CaSO_4 \rightarrow Ca_4Al_2(SO_4)(OH)_{12}\cdot 6H_2O + Ca(OH)_2$
C_2AH_8	$2Ca_2Al_2(OH)_{10}\cdot 3H_2O + CaSO_4 \rightarrow Ca_4Al_2(SO_4)(OH)_{12}\cdot 6H_2O + Ca(OH)_2 + 2\ Al(OH)_3$
CAH_{10}	$CaAl_2(OH)_8\cdot 2H_2O + CaSO_4 + 2Ca(OH)_2 \rightarrow Ca_4Al_2(SO_4)(OH)_{12}\cdot 6H_2O$
Strätlingite	$2Ca_2Al_2SiO_2(OH)_{10}\cdot 3H_2O + CaSO_4 \rightarrow Ca_4Al_2(SO_4)(OH)_{12}\cdot 6H_2O + 2SiO_2 + Ca(OH)_2 + 2\ Al(OH)_3$
Tricarboaluminate	$Ca_6Al_2(CO_3)_3(OH)_{12}\cdot 26H_2O + 3CaSO_4 \rightarrow Ca_6Al_2(SO_4)_3(OH)_{12}\cdot 26H_2O + 3CaCO_3$

Table 4
Dissolution reactions used to calculate solubility products

Mineral	Dissolution reaction
C_3AH_6	$Ca_3Al_2(OH)_{12} \rightarrow 3Ca^{2+} + 2AlO_2^- + 4OH^- + 4H_2O$
Siliceous hydrogarnet	$Ca_3Al_2(SiO_4)_{0.8}(OH)_{8.8} \rightarrow 3Ca^{2+} + 2AlO_2^- + 0.8HSiO_3^- + 3.2OH^- + 2.4H_2O$
Monosulfoaluminate	$Ca_4Al_2(SO_4)(OH)_{12}\cdot 6H_2O \rightarrow 4Ca^{2+} + 2AlO_2^- + SO_4^{2-} + 4OH^- + 10H_2O$
Monocarboaluminate	$Ca_4Al_2(CO_3)(OH)_{12}\cdot 5H_2O \rightarrow 4Ca^{2+} + 2AlO_2^- + CO_3^{2-} + 4OH^- + 9H_2O$
Hemicarboaluminate	$Ca_4Al_2(CO_3)_{0.5}(OH)_{13}\cdot 5.5H_2O \rightarrow 4Ca^{2+} + 2AlO_2^- + 0.5CO_3^{2-} + 5OH^- + 9.5H_2O$
C_4AH_{13}	$Ca_4Al_2(OH)_{14}\cdot 6H_2O \rightarrow 4Ca^{2+} + 2AlO_2^- + 6OH^- + 10H_2O$
C_2AH_8	$Ca_2Al_2(OH)_{10}\cdot 3H_2O \rightarrow 2Ca^{2+} + 2AlO_2^- + 2OH^- + 7H_2O$
CAH_{10}	$CaAl_2(OH)_8\cdot 6H_2O \rightarrow 2Ca^{2+} + 2AlO_2^- + 10H_2O$
Strätlingite	$Ca_2Al_2SiO_2(OH)_{10}\cdot 3H_2O \rightarrow 2Ca^{2+} + 2AlO_2^- + 1HSiO_3^- + OH^- + 7H_2O$
Tricarboaluminate	$Ca_6Al_2(CO_3)_3(OH)_{12}\cdot 26H_2O \rightarrow 6Ca^{2+} + 2AlO_2^- + 3CO_3^{2-} + 4OH^- + 30H_2O$
Ettringite	$Ca_6Al_2(SO_4)_3(OH)_{12}\cdot 26H_2O \rightarrow 6Ca^{2+} + 2AlO_2^- + 3SO_4^{2-} + 4OH^- + 30H_2O$
Jennite-type C–S–H	$Ca_{1.67}SiO_2(OH)_{3.33}\cdot 0.43H_2O \rightarrow 1.67Ca^{2+} + HSiO_3^- + 2.33OH^- + 0.43H_2O$
Tobermorite-type C–S–H	$Ca_{0.83}SiO_2(OH)_{1.67}\cdot 0.5H_2O \rightarrow 0.83Ca^{2+} + HSiO_3^- + 0.67OH^- + 0.5H_2O$

4.3. Solubility based estimation of standard molar thermodynamic properties

Explanation of the basic principles of the formulation, calculation and manipulation of solubility products is given in textbooks [24]. In the title paper, activity coefficients of the relevant species were calculated using the extended Debye–Hűckel Eq. (4):

$$\log\gamma_i = \frac{-Az_i^2\sqrt{I}}{1 + B\alpha_i\sqrt{I}} + bI \quad (4)$$

where γ_i is the activity coefficient of ion i, A and B are Debye–Hűckel solvent parameters dependent on the dielectric constant of water and temperature, z_i is the ionic charge, α_i is a parameter dependent on the size of ion, i, taken from [19,23]; b is a semi-empirical parameter (~0.064 at 25 °C) and I is the effective ionic strength. Aqueous ion activities and speciation were calculated using the GEMS database appropriate to the particular calculation. Finally, temperature-dependent solubility products were calculated from the activities obtained according to the dissolution reactions in

Table 4. The related Gibbs energy effect of reaction $\Delta_r G_T^0$ at temperature T was computed using Eq. (5):

$$\Delta_r G_T^0 = -RT\ln K_T \tag{5}$$

where R=8.31451 J/(molK) is the universal gas constant and K_T is a thermodynamic equilibrium constant (=equilibrium solubility product) at a given temperature.

From the solubility products calculated at each temperature, the standard molar thermodynamic properties of each solid were computed with the help of GEMS-PSI using the built-in three-term temperature extrapolation [28,29] to obtain a temperature-dependent "log K" function, which was fitted to the previously calculated solubility products. This function was estimated using Eq. (6) and the relationships shown in Eqs. (7–12).

$$\log K_T = A_0 + A_2 T^{-1} + A_3 \ln T \tag{6}$$

and

$$A_0 = \frac{0.4343}{R}\cdot\left[\Delta_r S_{T_0}^0 - \Delta_r Cp_{T_0}^0(1+\ln T_0)\right] \tag{7}$$

$$A_2 = -\frac{0.4343}{R}\cdot\left(\Delta_r H_{T_0}^0 - \Delta_r Cp_{T_0}^0 T_0\right) \tag{8}$$

$$A_3 = \frac{0.4343}{R}\cdot\Delta_r Cp_{T_0}^0 \tag{9}$$

$$\Delta_r S_T^0 = \Delta_r S_{T_0}^0 + \Delta_r Cp_{T_0}^0 \ln\frac{T}{T_0} \tag{10}$$

$$\Delta_r H_T^0 = \Delta_r H_{T_0}^0 + \Delta_r Cp_{T_0}^0 (T - T_0) \tag{11}$$

$$\Delta_r G_T^0 = \Delta_r H_T^0 - T\Delta_r S_T^0 \tag{12}$$

The heat capacity effect of reaction, $\Delta_r Cp_T{}^0 = \Delta_r Cp_{T0}^0 = \Delta a_o$, was assumed to be constant over the temperature range 0–100 °C. Two parameters were adjusted to obtain a best visual fit to the experimental data:

1) $\Delta_r G_T^0$ at the reference state (25 °C and 1 bar pressure) was estimated according to Eq. (5) using the experimentally derived solubility product at 25 °C.
2) $\Delta_r H_T^0$ at the reference state was estimated to obtain the best visual fit between extrapolated solubility products according to Eq. (6) and calculated solubility products from experimentally-derived solubilities.

$\Delta_r S^0 T$ was subsequently calculated using Eq. (12). Then the related standard molar thermodynamic properties were calculated according dissolution reactions given in (Table 4) using standard state properties of the aqueous species (Table 1) and the earlier estimated parameters $\Delta_r G^0 T$, $\Delta_r H^0 T$ and $\Delta_r S^0 T$. Combined with previously estimated Cp(T) coefficients (Table 2) and the known HKF parameters of the aqueous species, the individual temperature dependency of Cp_{T0} was subsequently calculated for each hydrate phase. Thus, in a final step, the solubility products were recalculated by GEMS using built-in parts of SUPCRT92 program [20] to derive temperature-dependent values. Differences arising between the first approach, using the three-term temperature extrapolation with assumed constant $\Delta_r Cp_T{}^0$, and the second calculation, taking into account temperature dependent heat capacity coefficients according to Table 2 and using values from the GEMS standard database [19,23], are marginal and lie within limits of other errors over the temperature range 0 to ~100 °C [28].

To check the internal consistency of the thermodynamic database, the experimentally-derived solubility data were predicted using the derived thermodynamic database and the observed phase assemblages. This seems like a circular argument and indeed is not intended to prove that the data are correct, only to demonstrate that internal self-consistency was achieved. The experimentally-derived solubility data for each phase are also listed in the title contribution, leaving the reader free to perform other calculations, if desired.

4.4. Solid solutions

Solid solutions are frequently encountered in cementitious systems. The molar Gibbs free energy ΔG_{ss} of a solution between different end members i can be calculated according to Eq. (13):

$$\Delta G_{ss} = \sum_i X_i \Delta_f G_i^0 + \Delta G_M \tag{13}$$

$$\Delta G_M = \Delta G_{id} + \Delta G_{ex} \tag{14}$$

$$\Delta G_{id} = RT\sum X_i \ln X_i \tag{15}$$

$$\Delta G_{ex} = RT\sum X_i \ln\gamma_i \tag{16}$$

The first term of Eq. (13) describes the free energy of a mechanical mixture of the end members i of the solid solution and is calculated using the mole fraction $X_i = n_i/\sum n_i$ (n_i is the mole amount of the end member i; $\sum X_i = 1$) and $\Delta_f G_i{}^0$ — the standard molar Gibbs energy of formation of end member i. The second term of Eq. (13) expresses the molar Gibbs energy of mixing, ΔG_M for a given composition of the solid solution series and is computed according to Eq. (14) as the sum of the Gibbs energy of mixing of an ideal solid solution, ΔG_{id}, and the excess Gibbs energy of mixing, ΔG_{ex}, for the solid solution. ΔG_{id} is calculated as described in Eq. (15) (with R, the universal gas constant, and T as the temperature of interest). The excess Gibbs energy of mixing, ΔG_{ex}, is only needed to compute thermodynamic properties of non-ideal solid solutions and can be calculated according to Eq. (16), where γ_i is the activity coefficient of the end member i. In the case of an ideal solid solution, all γ_i equal 1 and thus $\Delta G_{ex} = 0$. In the title study,

an ideal solid solution model ($\Delta G_{ex}=0$) was used to describe the thermodynamic properties of single phase calcium–silicate–hydrate (C–S–H). A more detailed explanation of this solid solution model can be found in [30].

Several cementitious phases form non-ideal solid solutions, but only over a limited range of compositions. Hence, miscibility gaps will be observed. In the case of non-ideal mixing the Gibbs energy of the solid solution, ΔG_{ss}, is calculated with Eq. (13) and the activity coefficients $\gamma_i \neq 1$ and the excess Gibbs energy of mixing, ΔG_{ex}, of a binary solid solution are calculated according to Eq. (17):

$$\Delta G_{ex} = RT(X_1 \ln\gamma_1 + X_2 \ln\gamma_2) \quad (17)$$

where $X_1=n_1/(n_1+n_2)$ and $X_2=n_2/(n_1+n_2)$ (n_1 and n_2 are the amounts of end members; $X_1+X_2=1$).

The GEMS-PSI code has several built-in functions for non-ideal solid solutions [31]. In the title paper, we use a semi-empirical model first suggested by Guggenheim and later developed by Redlich and Kister [31,32] to estimate the excess Gibbs free energy function of a non-ideal binary solid solutions Eq. (18):

$$\Delta G_{ex} = X_1 X_2 RT\left(a_0 + a_1(X_1 - X_2) + a_2(X_1 - X_2)^2 + \ldots\right) \quad (18)$$

The empirical interaction parameters a_0, a_1, … are dimensionless. As shown by Glynn [32], knowledge of two fitting parameters a_0 and a_1 is sufficient to estimate the excess Gibbs energy function with reasonable accuracy. The activity coefficients γ_i of the end members i can be derived by fitting a_0 and a_1 to Eq. (18) and estimated according Eqs. (19) and (20):

$$\ln\gamma_1 = X_2^2[a_0 + a_1(3X_1 - X_2)] \quad (19)$$

$$\ln\gamma_2 = X_1^2[a_0 - a_1(3X_2 - X_1)] \quad (20)$$

In the title study, the software MBSSAS [32] was used to derive the fitting parameters a_0 and a_1 based on experimentally-observed compositional boundaries of the miscibility gap in the binary solid solution series. A detailed description of MBSSAS is given in [32]: Kersten [33] applied a similar approach to estimate thermodynamic data for C–S–H.

5. Results

Table 2 summarises all thermodynamic data obtained in this study as well as thermodynamic data of supplementary phases needed to estimate the data of the cement hydrates. The following paragraphs explain in detail the determination of standard molar thermodynamic properties of the individual cement hydrates.

5.1. Hydrogarnet

5.1.1. C_3AH_6, $Ca_3Al_2(OH)_{12}$

As shown in Fig. 2, no significant changes of mineralogy occurred in the temperature range from 25 °C to 105 °C amongst the solid samples commencing from undersaturation: C_3AH_6 was the only crystalline phase detected by XRD. However at 5 °C small amounts of C_2AH_8 and monocarboaluminate were present. Whereas the formation of monocarboaluminate is an artefact, probably due to CO_2 contamination of the sample during preparation, formation of C_2AH_8 seems to be favoured at low temperatures. Table 5 shows the results of the solubility experiments for C_3AH_6; the solubilities of calcium and aluminium remain little-changed over the range studied. Thus the observed decrease of pH with rising temperature results mainly from the temperature-dependent change of the ion product of water. The mean aqueous ratios of Ca:Al, ~3: 2, indicate congruent dissolution; comparable solubilities derived from super- and undersaturation are very similar. No significant solubility changes occurred between 28 and 84 days, suggesting that a steady state was reached within 28 days.

Fig. 3 shows the evolution of calculated solubility products using solubility data from different sources including those obtained in the title study. In the low temperature range, from 0–50 °C, considerable data scatter is apparent. Although apparently comparable experimental conditions were used, older solubility data published by Wells et al. [17,34] and by D'Ans

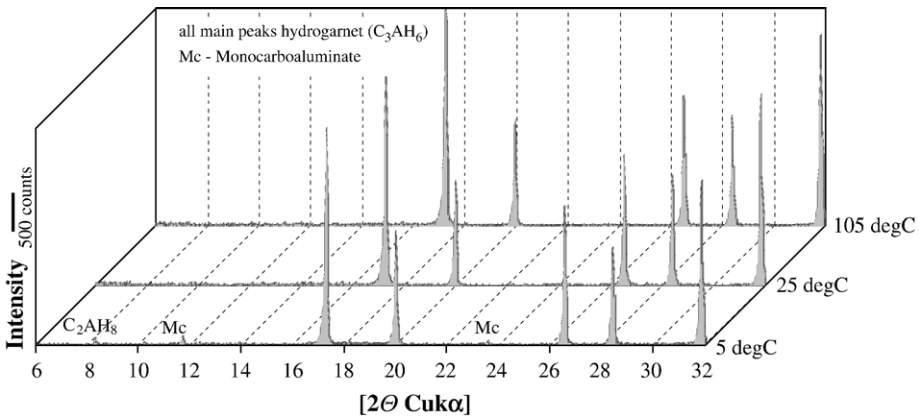

Fig. 2. Comparison of XRD-patterns of C_3AH_6 following annealing at 5, 25 and 105 °C (approach from undersaturation).

Table 5
Solubility data for C_3AH_6 at different temperatures and ages

Age	Temperature	Ca	Al	pH	Log_K_{sp}	Phases
[Day]	[°C]	[mmol/l]	[mmol/l]			
C_3AH_6 (samples cooled down from initially ~105 °C)						
28	5	6.57	4.17	12.63	−20.59	n.d.
56	5	7.20	4.10	12.68	−20.29	n.d.
84	5	7.11	4.77	12.65	−20.31	C_3AH_6, C_2AH_8, C_4AcH_{11}
28	25	6.91	4.24	11.91 (11.98[1])	−20.52	n.d.
56	25	7.29	4.80	11.92 (11.90[2])	−20.34	n.d.
84	25	6.31	5.07	11.81 (11.79[3])	−20.84	C_3AH_6
28	55	6.66	4.20	11.01	−20.91	n.d.
56	55	6.87	4.59	11.01	−20.80	n.d.
84	55	7.01	4.90	11.01	−20.73	C_3AH_6
56	70	6.34	4.44	10.60	−21.25	n.d.
84	70	6.39	4.24	10.62	−21.22	C_3AH_6
28	85	5.73	3.64	10.27	−21.80	n.d.
56	85	6.18	4.39	10.27	−21.55	n.d.
84	85	6.19	4.60	10.26	−21.55	C_3AH_6
28	105	5.64	3.44	9.89	−22.22	n.d.
56	105	5.70	3.76	9.88	−22.17	n.d.
84	105	5.81	4.44	9.85	−22.11	C_3AH_6
C_3AH_6 (from undersaturation)						
28	5	6.79	4.63	12.62	−20.47	n.d.
56	5	7.03	5.07	12.64	−20.36	n.d.
84	5	7.01	4.40	12.65	−20.37	C_3AH_6, C_2AH_8
28	25	7.20	4.73	11.91 (11.96[1])	−20.38	n.d.
56	25	7.34	4.55	11.93 (11.90[2])	−20.32	n.d.
84	25	7.31	3.94	11.95 (11.91[3])	−20.36	C_3AH_6
28	55	6.93	4.33	11.03	−20.78	n.d.
56	55	6.84	4.04	11.03	−20.83	n.d.
84	55	7.16	4.44	11.04	−20.68	C_3AH_6
56	70	6.39	3.97	10.63	−21.23	n.d.
84	70	6.31	4.37	10.61	−21.26	C_3AH_6
28	85	6.15	4.14	10.28	−21.57	n.d.
56	85	6.13	3.88	10.29	−21.59	n.d.
84	85	6.11	4.27	10.27	−21.59	C_3AH_6
28	105	5.57	3.67	9.87	−22.24	n.d.
56	105	5.63	4.46	9.83	−22.21	n.d.
84	105	5.66	4.07	9.86	−22.19	C_3AH_6

[1]Temperature of solution 24 °C at time of measurement [2] temperature of solution 26 °C at time of measurement [3] temperature of solution 25 °C at time of measurement.

et al. [35] differ significantly from those obtained in the title study. On the other hand, the solubility products calculated from other available solubility data [12,15,37–40] agree well with our dataset within analytical accuracies (see Table 5).

The resulting standard molar thermodynamic properties of C_3AH_6 are summarised in Table 2. Our data agree well with those reported by Babushkin et al. [1] ($\Delta_f G^0 = -5014.1$ kJ/mol, $\Delta_f H^0 = -5548$ kJ/mol). $\Delta_f H^0$ as well as with experimentally determined data by Berman [41] ($\Delta_f H^0 \sim -5561$ kJ/mol) and Schoenitz et al. [42] ($\Delta_f H^0 \sim -5551.5$ kJ/mol): all lie within the expected range of analytical errors.

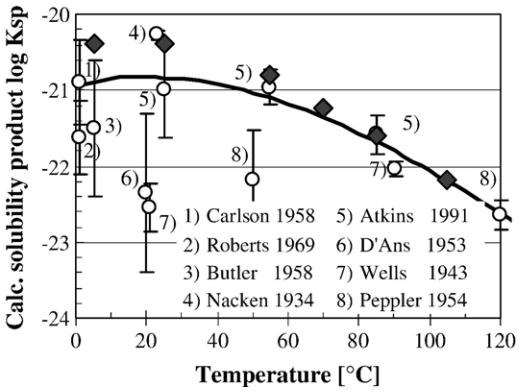

Fig. 3. Calculated solubility products of C_3AH_6 from solubility experiments (lines show calculated results as best fit).

Fig. 4 shows the recalculated temperature-dependence of calcium and aluminium solubilities from C_3AH_6 redispersed in pure water using the experimental conditions described in paragraph 3.3. The calculated data show good agreement with averaged measured solubilities. Consideration of other solubility data (see Fig. 3), especially values at lower temperatures, show slightly lower solubilities compared to the data obtained in the title paper. Hydrogarnet was predicted as the only stable $CaO–Al_2O_3–H_2O$ solid over the temperature range from 5 to 100 °C at 1 bar pressure.

5.1.2. Siliceous hydrogarnet, $Ca_3Al_2(SiO_4)_{0.8}(OH)_{8.8}$

As shown in Fig. 5, phase pure siliceous hydrogarnet could not be synthesized using the procedure described in 3.2.1. Small amounts of a C–S–H phase, coprecipitated during the initial synthesis of siliceous hydrogarnet, persisted at all temperatures between 5–85 °C despite three dispersions in the course of solubility experiments. As noted in Section 3.2.1, it is probable that the siliceous hydrogarnet had a lower silicon content than the target. Thus provisional solubility products were calculated using the composition estimated from XRD data, $Ca_3Al_2(SiO_4)_{0.8}(OH)_{8.8}$.

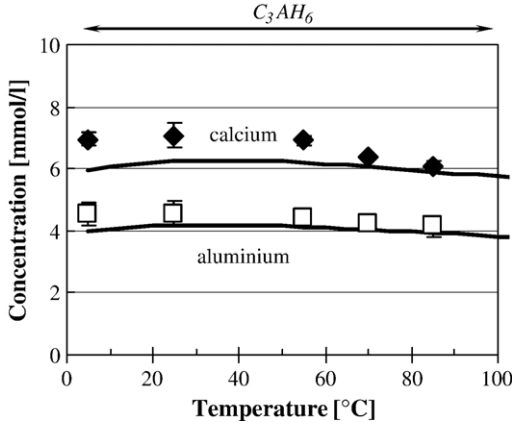

Fig. 4. Recalculated solubility data for hydrogarnet, C_3AH_6, based on fitted thermodynamic data from Fig. 3 (markers show experimental values from the title study; lines show calculated results).

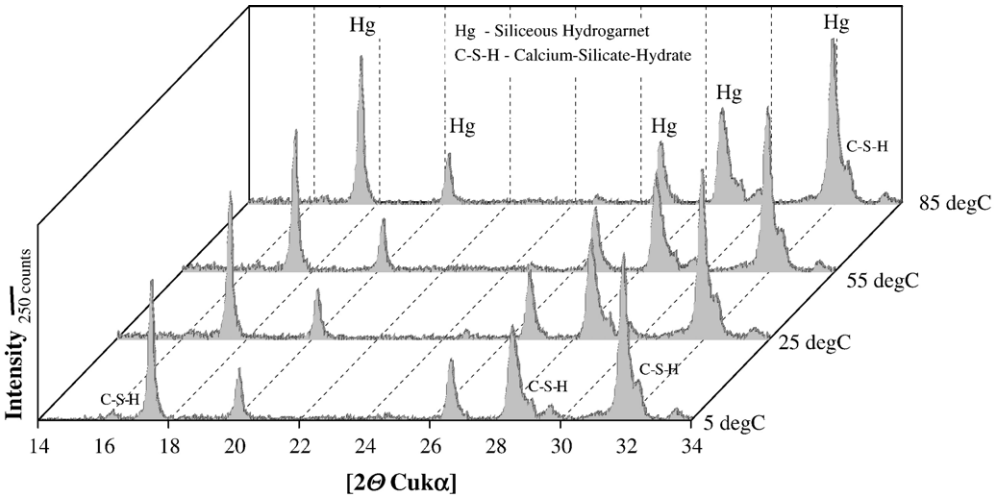

Fig. 5. Comparison of XRD-patterns of siliceous hydrogarnet following ageing at temperatures in the range 5–85 °C (approach from undersaturation).

Table 6 shows provisional solubility data for the siliceous hydrogarnet. Comparison with the C_3AH_6 data shows that silicon substitution leads to a significant reduction of solubility, indicating stabilisation of the hydrogarnet phase by silicon substitution. The calculated solubility products of siliceous hydrogarnet are considerably lower than those of C_3AH_6.

As shown in Table 6, small amounts of sodium were also present in the aqueous solution. The amount of sodium in the solution diminished with each extraction and successive redispersion suggesting that the sodium is mainly adsorbed in the C–S–H hydrate phase and is probably not structurally incorporated in the garnet-structured hydrate. C–S–H -present as impurity- is known to bind sodium weakly [43] and the equilibrium with dissolved sodium also influences the pH of the solution. Nevertheless, concentrations of other relevant ions remained generally constant. Thus the apparent decrease of the solubility product with each new extraction at a given temperature is mainly attributed to a lowered hydroxide activity due to decreasing aqueous sodium concentrations.

Fig. 6 shows a comparison of experimentally derived, temperature-dependent solubility products for siliceous hydrogarnet, $Ca_3Al_2(SiO_4)_{0.8}(OH)_{8.8}$. The fitted values are calculated from the data in Table 2. There is a lack of consistent data for siliceous hydrogarnet; the only previous solubility data for siliceous hydrogarnet were published by Atkins et al for 25 °C [12] and Jappy et al. [11] for 95 °C. These investigations [11,12] apparently used preparations with two coexisting hydrogarnet phases and it is not therefore possible to compare these data directly with those obtained in the title study. Nevertheless the solubility trends given for siliceous hydrogarnets with high silicon contents [11,12] generally agree with those of the title study; the greater the substitution of silicon in hydrogarnet, the lower the solubility.

Table 6
Solubility data of siliceous hydrogarnet ($C_3AS_{0.8}H_{4.4}$) at different temperatures

$C_3AS_{0.8}H_{6.4}$ (from undersaturation[1])							
Temperature	Ca	Al	Si	Na	pH	Log_K_{sp}	Phases
[°C]	[mmol/l]	[mmol/l]	[mmol/l]	[mmol/l]			
5	0.46	0.29	0.10	0.83	11.84	−30.05	n.d.
5	0.52	0.23	0.08	0.35	11.75	−30.42	n.d.
5	0.48	0.22	0.06	0.20	11.65	−30.90	$C_3AS_{0.8}H^3_{4.4}$, C–S–H
25	0.56	0.26	0.11	0.87	11.19 (11.13[2])	−29.58	n.d.
25	0.55	0.24	0.10	0.30	11.00 (10.94[2])	−30.22	n.d.
25	0.57	0.26	0.08	0.17	10.97 (10.90[2])	−30.29	$C_3AS_{0.8}H^3_{4.4}$, C–S–H
55	0.72	0.28	0.15	0.96	10.41	−28.94	n.d.
55	0.72	0.29	0.16	0.26	10.23	−29.43	n.d.
55	0.70	0.30	0.17	0.13	10.16	−29.64	$C_3AS_{0.8}H^3_{4.4}$, C–S–H
70	0.70	0.33	0.18	0.87	10.02	−28.97	n.d.
70	0.67	0.30	0.18	0.26	9.84	−29.64	n.d.
70	0.65	0.34	0.17	0.10	9.74	−29.90	$C_3AS_{0.8}H^3_{4.4}$, C–S–H.
85	0.67	0.30	0.18	0.87	9.72	−29.22	n.d.
85	0.62	0.30	0.19	0.30	9.52	−29.87	n.d.
85	0.60	0.31	0.22	0.16	9.43	−30.14	$C_3AS_{0.8}H^3_{4.4}$, C–S–H

[1]All samples analysed after 4 week stored at the given temperature. After each analysis the removed solution (~20 ml) was replaced with ultrapure degassed water.
[2]Temperature of solution 26 °C at time of measurement [3]estimated composition.

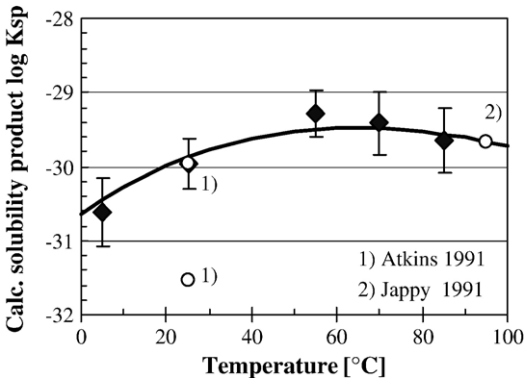

Fig. 6. Calculated solubility products of siliceous hydrogarnet, $C_3AS_{0.8}H_{4.4}$, from solubility experiments (lines show best fit to the calculated results).

A comparison of experimentally-derived solubilities of $C_3AS_{0.8}H_{4.4}$ with modelled values is demonstrated in Fig. 7, to prove the solubility experiments. Small concentrations of sodium were determined in the solubility experiments and, to enable a direct relation with the experimental values, 0.4 mmol sodium/kg water were arbitrarily added to the model solution to simulate the impact of sodium on $C_3AS_{0.8}H_{4.4}$ solubility. While the aluminium concentrations are slightly overestimated by calculation, data for calcium and silicon show good agreement with the averaged measured solubilities. $C_3AS_{0.8}H_{4.4}$ is computed to be the only stable solid at this composition between 5 to 100 °C.

5.2. AFm-phases

5.2.1. Monosulfoaluminate, $Ca_4Al_2(SO_4)(OH)_{12}\cdot 6H_2O$

Monosulfoaluminate preparations give apparently single phase preparations with relatively coarse hexagonal plate morphology (see Fig. 8a). As shown in Fig. 9, monosulfoaluminate was the dominant phase at all temperatures. However after redispersion at 5 °C, 25 °C and 50 °C, small amounts of ettringite developed (see Fig. 8b). Additionally, small amounts of hemicarboaluminate were formed in several samples

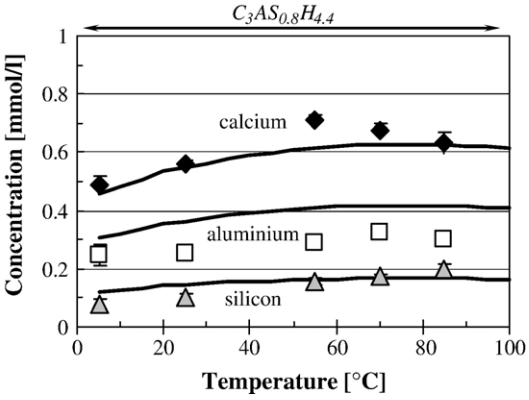

Fig. 7. Recalculated solubility data for hydrogarnet, $C_3AS_{0.8}H_{4.4}$, based on fitted thermodynamic data from Fig. 6 (markers show experimental values from this study; lines show calculated trends).

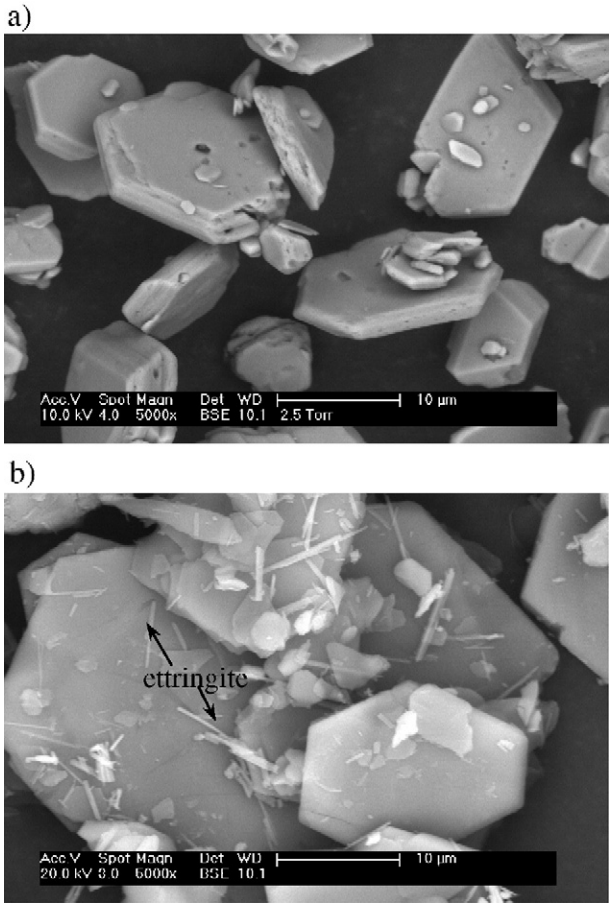

Fig. 8. SEM micrographs of synthetic monosulfoaluminate a) after synthesis at 85 °C and b) after 4 weeks redispersion in deionised water at 25 °C.

indicating minor CO_2 contamination during sample preparation and treatment. No mineralogical changes were observed in a sample stored at 25 °C for 14 months. Despite the supposed metastability of monosulfoaluminate with respect to hydrogarnet and ettringite, C_3AH_6 was generally absent except at 5 °C; see below.

Temperature-dependent solubility data for monosulfoaluminate are compiled in Table 7. Calcium and aluminium solubilities remained relatively constant over the temperature range investigated. Although the aqueous ratios of Ca: Al (~4: 1.3–1.9) are close to congruency the Ca: SO_4 ratio (~500) differs significantly from congruent dissolution behaviour up to ~25 °C. This incongruent solubility behaviour was reported by Atkins et al. [12], whose solubility data at 25 °C agree very well with those of the title study. Nevertheless, with rising temperatures, the dissolution of monosulfoaluminate approaches congruency; sulfate concentrations increase significantly between 25 and 70 °C. At higher temperatures, ≥70 °C, monosulfoaluminate dissolves congruently.

An exception to the lack of C_3AH_6 formation is the experiment at 5 °C, with approach from supersaturation. Significant amounts of C_3AH_6 formed and solubility values derived from this experiment differ significantly from other supposedly comparable data. Therefore this data set was not used in the title paper (see Table 7).

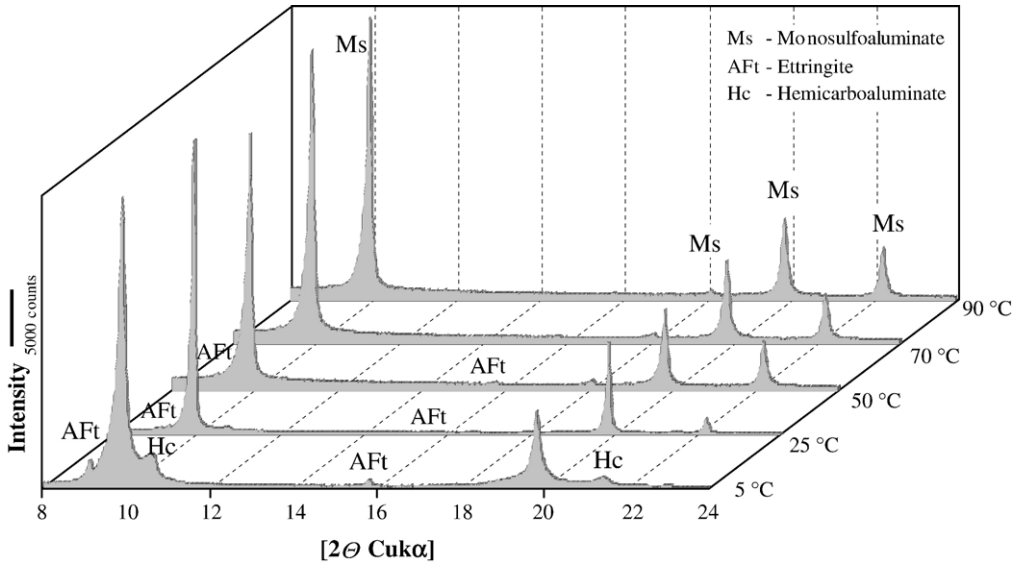

Fig. 9. Comparison of XRD-patterns of monosulfoaluminate after ageing at temperatures in the range 5–90 °C (approach from undersaturation).

Although the application of the solubility product concept to phases showing incongruent dissolution is problematical, solubility products were nevertheless calculated according to Table 7. The averaged temperature-dependent solubility products were used to estimate the standard molar thermodynamic properties of monosulfoaluminate. A comparison between the fitted solubility product curve and calculated values from other data sources [12,15,45–48] shows good agreement within the range of possible analytical errors (Fig. 10). Only the solubility product calculated from solubility data by D'Ans et al. [36] is significantly higher than our fit. The estimated data from the title study ($\Delta_f G^0 \sim -7778.5$ kJ/mol, $\Delta_f H^0 \sim -8750$ kJ/mol, S^0 821 J/mol K) agree well with the dataset published by Babushkin et al. [1] ($\Delta_f G^0 \sim -7779$ kJ/mol, $\Delta_f H^0 \sim -8772$ kJ/mol, S^0 747 J/mol K) and reasonably well with data obtained by Satava [51] ($\Delta_f G^0 \sim -7732$ kJ/mol, $\Delta_f H^0 \sim -8712$ kJ/mol, $S^0 \sim 791$ J/mol K); estimated values for $\Delta_f H^0$ are slightly less than experimental data from dissolution calorimetry reported by Berman [49] ($\Delta_f H^0 \sim -8786$ kJ/mol).

To test the consistency of the derived dataset, experimental solubility data were recalculated using standard thermodynamic properties of the minerals given in Table 2; Fig. 11 shows that calculated and experimental values exhibit very good agreement in the temperature range between 25 and 100 °C. Only values

Table 7
Solubility data of nominally monosulfoaluminate(C_4AsH_{12}) at temperatures 5–100 °C

C_4AsH_{12}								
Age	Temperature		Ca	Al	SO_4^{2-}	pH	Log_K_{sp}	Phases
[Day]	[°C]		[mmol/l]	[mmol/l]	[mmol/l]			
42	5	us	4.70	2.92	0.005	12.49	−29.92	C_4AsH_{12}, AFt, $C_4Ac_{0.5}H_{11.5}$
42	5	ss	14.6	<0.02	9.300	12.63	n.d.	C_4AsH_{12}, AFt, $C_4Ac_{0.5}H_{11.5}$, C_3AH_6
28	25	ss	5.51	2.91	0.009	11.84 (11.90[1])	−29.24	C_4AsH_{12}, AFt
56	25	ss	5.06	3.13	0.009	11.79 (11.83[1])	−29.48	C_4AsH_{12}, AFt
84	25	ss	5.14	3.29	0.010	11.77 (11.82[1])	−29.43	C_4AsH_{12}, AFt
450	25	ss	5.01	3.71	0.012	11.73 (11.77[1])	−29.43	C_4AsH_{12}, AFt, Hc
28	25	us	4.87	3.93	0.014	11.71 (11.70[2])	−29.44	C_4AsH_{12}, AFt
56	25	us	4.95	3.42	0.011	11.75 (11.80[1])	−29.45	C_4AsH_{12}, AFt, $C_4Ac_{0.5}H_{11.5}$
56	40	us	3.95	3.31	0.240	11.10	−29.26	C_4AsH_{12}, AFt
42	50	us	4.40	2.84	0.398	10.91	−28.84	C_4AsH_{12}, AFt[3)]
42	50	ss	4.49	2.64	0.253	10.97	−28.86	C_4AsH_{12}, AFt
56	65	us	4.09	3.13	0.520	10.44	−29.29	n.d.
42	70	ss	4.88	2.57	1.264	10.37	−28.79	C_4AsH_{12}, AFt[3)]
42	70	us	4.37	2.18	1.053	10.36	−29.17	C_4AsH_{12}
56	85	us	4.62	2.63	1.310	9.99	−29.33	n.d.
42	90	ss	5.19	2.57	1.788	9.91	−29.12	C_4AsH_{12}
42	90	us	5.19	1.87	2.333	9.87	−29.47	C_4AsH_{12}
56	100	us	4.45	2.67	1.510	9.62	−29.86	n.d.

[1]measured at 24 °C, [2]measured at 25 °C [3]very weak signal. Abbreviations: us — undersaturation, ss — supersaturation.

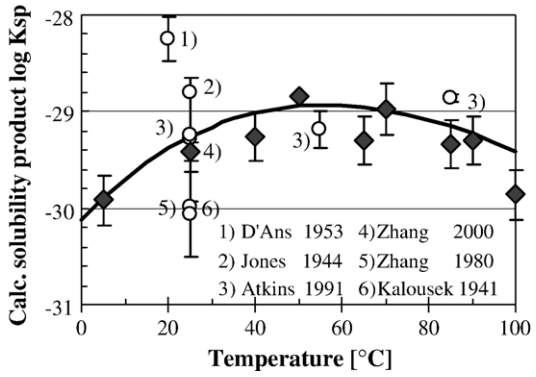

Fig. 10. Calculated solubility products of monosulfoaluminate from solubility experiments (line shows calculated best fit).

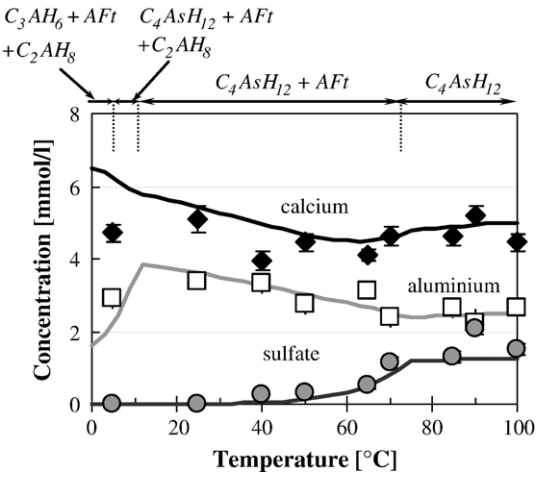

Fig. 11. Recalculated solubility data for nominally monosulfoaluminate based on fitted thermodynamic data from Fig. 10 (markers show experimental values from the title study; lines show calculated results).

obtained at 5 °C from analyses from undersaturation differ significantly from the trend lines. It is interesting to note that, as indicated in Fig. 11, monosulfoaluminate is predicted to appear as a stable phase at temperatures >5 °C in the system $CaO–Al_2O_3–CaSO_4–H_2O$ using the revised values for hydrogarnet, C_3AH_6. Coprecipitation of small amounts of AFt is predicted to occur at temperatures ≤~70 °C and its formation was indeed observed in our experiments. This indicates that coprecipitation of AFt and monosulfoaluminate lowers total Gibbs energy of the system and is energetically favourable. Formation of small amounts of AFt has been reported by several authors who tried to synthesize monosulfoaluminate at ~25 °C by adding stoichiometric amounts of calcium, aluminium and sulfate [12,36,46]. Nevertheless, and in agreement with our calculations, formation of hydrogarnet was not observed. According to calculations by Damidot et al. [44,50] monosulfoaluminate is metastable with respect to a mixture of C_3AH_6 and ettringite at temperatures below ~50 °C. These calculations used thermodynamic data derived from C_3AH_6 solubilities given by Wells et al. [17]. But according to the title study, monosulfoaluminate will be stable at and below room temperature, decomposing to a mixture of C_2AH_8, C_3AH_6 and ettringite at ≤~5 °C. Additionally, at temperatures <~10 °C, C_2AH_8 is calculated to precipitate.

5.2.2. Monocarboaluminate, $Ca_4Al_2(CO_3)(OH)_{12}\cdot 5H_2O$

Fig. 12 shows that the XRD-pattern of monocarboaluminate remained unchanged at temperatures ≤70 °C, confirming its stability. Monocarboaluminate and small amounts of calcite were observed as crystalline phases after 6 weeks storage at ≤70 °C. As shown in Fig. 12, monocarboaluminate decomposes to a mixture of C_3AH_6 and $CaCO_3$ at temperatures ≥90 °C. But weak X-ray reflections of monocarboaluminate persisted and are interpreted as indicating that equilibrium may not have been reached.

Until recently, solubility data for monocarboaluminate were only available at 25 °C [52–54]. Thus an important target of this study was to extend the known dataset to other temperatures: these data are given in Table 8. Monocarboaluminate is incongruently soluble: the estimated aqueous calcium: carbonate ratios (Ca^{2+}:CO_3^{2-} >300) differ greatly from congruency.

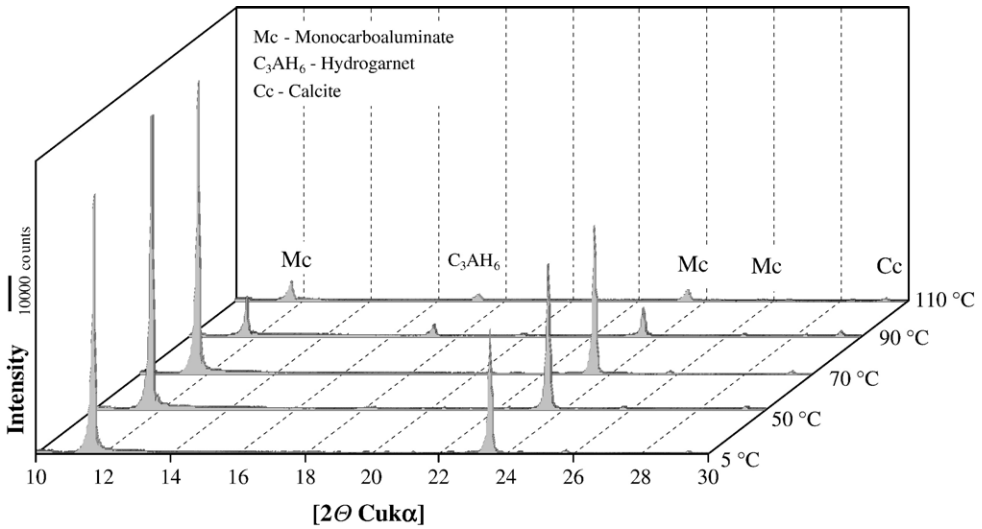

Fig. 12. Comparison of XRD-patterns of monocarboaluminate after annealing at temperatures in the range 5–110 °C (approach from undersaturation).

Table 8
Solubility data of monocarboaluminate (C_4AcH_{11}) at temperatures 5–110 °C

C_4AcH_{11}								
Age	Temperature		Ca	Al	CO_3^{2-} [1]	pH	Log_K_{sp}	Phases
[Day]	[°C]		[mmol/l]	[mmol/l]	[mmol/l]			
42	5	us	2.58	1.60	0.008	12.24	−32.28	C_4AcH_{11}, Calcite
42	5	us	2.52	1.56	0.008	12.24	−32.36	n. d.
42	5	us[2]	2.35	1.63	0.008	12.18	−32.60	C_4AcH_{11}, Calcite
56	25	us	3.19	2.32	0.008	11.56 (11.59[3])	−31.66	C_4AcH_{11}, Calcite
84	25	ss	3.73	2.16	0.008	11.67 (11.62[3])	−31.12	C_4AcH_{11}, Calcite
42	50	us	4.42	2.34	0.007	11.01	−30.94	C_4AcH_{11}, Calcite
42	50	us	4.46	2.51	0.007	11.00	−30.89	n. d.
42	50	us[2]	4.30	2.40	0.007	10.99	−31.02	C_4AcH_{11}, Calcite
42	70	us	5.24	3.30	0.007	10.56	−30.78	C_4AcH_{11}, Calcite
42	70	us	5.35	3.42	0.007	10.56	−30.71	n. d.
42	70	us[2]	5.11	2.94	0.007	10.56	−30.88	C_4AcH_{11}, Calcite
42	90	us	6.54	5.02	0.006	10.17	n. d.	$C_4AcH_{11}^{4}$, Calcite, C_3AH_6.
42	110	us	6.05	4.56	0.005	9.78	n. d.	$C_4AcH_{11}^{4}$, Calcite, C_3AH_6.

[1]Calculated values assuming equilibrium with calcite [2]prepared from a stoichiometric mixture of $Al(OH)_3$, $CaCO_3$ and CaO in 0.1 mol KOH-solution at 50 °C [3]measured at 25 °C [4]weak signals. Abbreviations: us — undersaturation, ss — supersaturation.

Carbonate concentrations were always below the detection limit of the analytical technique (<~0.1 mmol/l CO_3^{2-}). Thus a direct determination of carbonate solubility was not possible. Other authors report the same analytical problem[52–54]. To enable calculation of solubility products, carbonate solubilities were computed assuming a saturation of the supernatant with respect to calcite. This is justified, as small amounts of calcite were found as a supernumerary phase in all analyses.

A comparison of the solubility product from the title study with other values calculated from solubility data [16,53,54], demonstrates good data consistence for monocarboaluminate at 25 °C (Fig. 13). Only the equilibrium constants computed from solubility data by Zhang [47] and Nishikawa [52] are slightly lower than those of the title study. As shown in Table 8 and Fig. 14, calcium and aluminium concentrations increase regularly to about 90 °C; the 110 °C value apparently decreases slightly. Calculated solubility curves based on the new dataset (Table 2) reproduce well the experimentally-determined values. In agreement with the XRD analysis, (Fig. 12), monocarboaluminate is predicted to decompose at temperatures >~85 °C to mixtures of C_3AH_6 and calcite. Kuzel and Baier [55] investigated the hydration of calcium aluminate cements in the presence of calcium carbonate at elevated temperatures and found similar results, suggesting that the solid phase assemblage of gibbsite-monocarboaluminate is stable up to 90±5 °C.

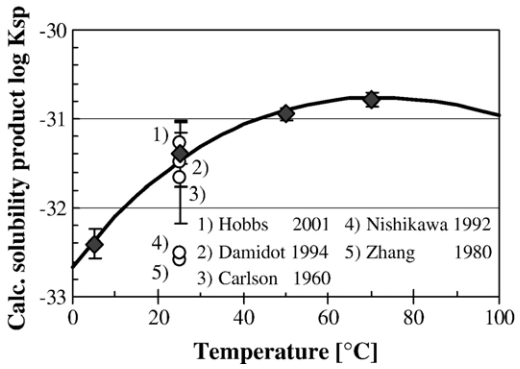

Fig. 13. Calculated solubility products of monocarboaluminate from solubility experiments (line shows calculated best fit).

5.2.3. Hemicarboaluminate, $Ca_4Al_2(CO_3)_{0.5}(OH)_{13}\cdot 5.5H_2O$

Although its existence has been known since the 1960's [56,57], hemicarboaluminate is one of the least well characterised AFm-phases. Damidot et al. [54] published the first thermodynamic data for this compound showing it to be incompatible with calcite. Despite its suggested lack of importance in "real" systems saturated with respect to calcite [58], investigations by Kuzel et al. [59,60] and recent calculations by Matschei et al. [61,62] predict that hemicarboaluminate will be encountered in OPC with very low carbonate contents (i.e. virtually "carbonate-free" cements). Until recently, no temperature-dependent data for the stability of hemicarboaluminate were available. As shown in Fig. 15, the intensities of

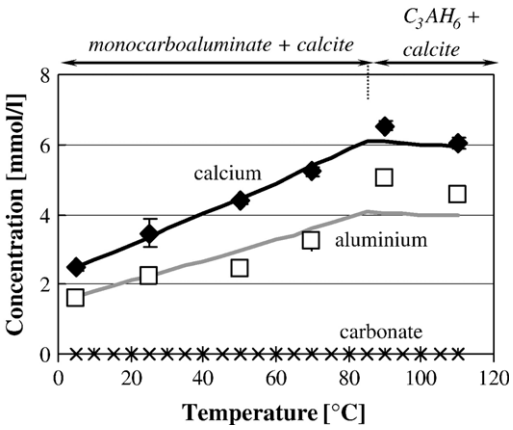

Fig. 14. Recalculated solubility data for nominally monocarboaluminate based on fitted thermodynamic data from Fig. 13; (markers show experimental values from the title study, lines show calculated fit). Predicted solid phases are shown at the top.

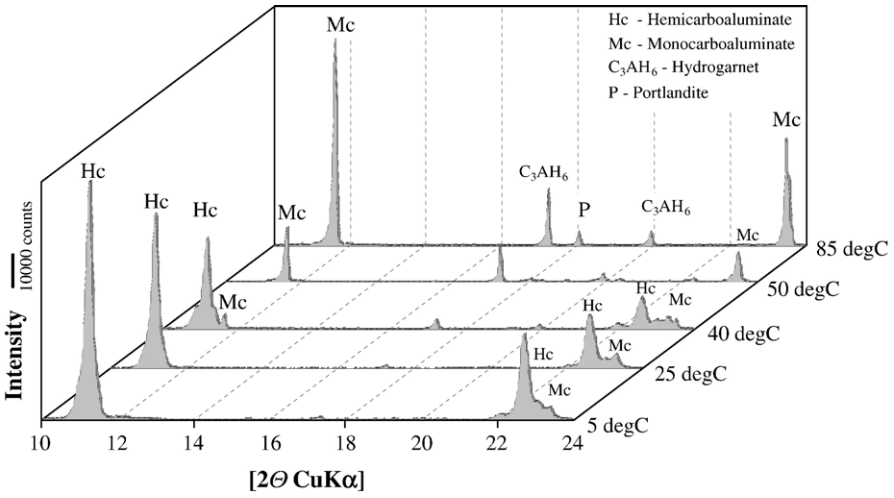

Fig. 15. Comparison of XRD-patterns of nominally hemicarboaluminate after ageing at temperatures in the range 5–85 °C (approach from undersaturation).

the XRD-reflections of hemicarboaluminate decrease regularly over the temperature range between 5° and 40 °C while at the same time, those of C_3AH_6 and monocarboaluminate increase in intensity in the range 5°–40 °C. But hemicarboaluminate was absent at both 50 °C and 85 °C and the phase constitution was instead dominated by the coexistence of monocarboaluminate, C_3AH_6 and portlandite.

Solubilities of hemicarboaluminate were obtained from super- and undersaturated solutions; the results are shown in Table 9. The resulting calculated solubility products, Table 9, were used to fit the standard thermodynamic properties of the compound (Fig. 16 and Table 2). The amounts of dissolved carbonate were always below the detection limit of the analytical technique but in this instance, carbonate concentrations could not be calculated by assuming calcite saturation because hemicarboaluminate is not stable in the presence of calcite. But, since XRD-investigations showed hemicarboaluminate to be compatible with monocarboaluminate, saturation with respect to the latter was assumed and used to calculate carbonate concentrations.

Hemicarboaluminate solubilities are strongly incongruent. As can be seen in Fig. 17, calcium concentrations increase with increasing temperatures to ~50 °C, at and above which hemicarboaluminate is predicted to be unstable. The derived solubility products from this study agree reasonably well with values calculated from solubility data by Hobbs et al. [53] (using carbonate concentrations estimated by assuming monocarboaluminate saturation) and by Damidot et al. [54]. Hemicarboaluminate decomposes progressively with increasing temperatures. As calculated (Fig. 18), and in agreement with XRD–Analyses (Fig. 15), the amount of hemicarboaluminate decreases regularly with increasing temperatures while

Table 9
Solubility data of nominally hemicarboaluminate ($C_4Ac_{0.5}H_{12}$) at temperatures 5–85 °C

$C_4Ac_{0.5}H_{12}$								
Age	Temperature		Ca	Al	CO_3^{2-} [1]	pH	Log_K_{sp}	Phases
[Day]	[°C]		[mmol/l]	[mmol/l]	[mmol/l]			
28	5	ss	8.01	1.19	2.1E-06	12.84	−29.67	$C_4Ac_{0.5}H_{11.5}$, C_4AcH_{11}, C_3AH_6
56	5	us	7.21	0.81	8.2E-06	12.80	−30.01	$C_4Ac_{0.5}H_{11.5}$, C_4AcH_{11}, C_3AH_6.
28	25	ss	13.08	0.12	1.5E-04	12.32 (12.31[2])	−29.35	$C_4Ac_{0.5}H_{11.5}$, C_4AcH_{11}, C_3AH_6
56	25	us	11.43	0.40	3.3E-05	12.26 (12.24[2])	−29.08	$C_4Ac_{0.5}H_{11.5}$, C_4AcH_{11}, C_3AH_6
28	25	ss	11.32	0.48	2.1E-05	12.25 (12.27[2])	−29.00	$C_4Ac_{0.5}H_{11.5}$, C_4AcH_{11}, C_3AH_6
28	25	us	10.48	0.49	3.4E-05	12.22 (12.22[2])	−29.14	n.d.
365	25	us	9.55	0.80	2.3E-05	12.18 (12.30[3])	−29.12	$C_4Ac_{0.5}H_{11.5}$, C_3AH_6
28	40	ss	15.02	0.20	1.4E-04	11.90	−28.82	n.d.
56	40	us	12.81	0.41	8.4E-05	11.83	−28.79	$C_4Ac_{0.5}H_{11.5}$, C_4AcH_{11}, C_3AH_6
28	50	ss	16.03	0.31	1.2E-04	11.64	n. d.	C_4AcH_{11}, C_3AH_6, $Ca(OH)_2$
56	50	us	17.02	0.30	9.2E-05	11.67	n. d.	C_4AcH_{11}, C_3AH_6
28	70	ss	10.31	0.62	1.3E-03	10.97	n. d.	n.d.
56	70	us	12.39	0.45	1.6E-03	10.97	n. d.	C_4AcH_{11}, C_3AH_6
28	85	ss	12.02	0.53	3.1E-03	10.71	n. d.	C_4AcH_{11}, C_3AH_6, $Ca(OH)_2$
56	85	us	10.53	0.62	1.1E-03	11.04	n. d.	n.d.
84	85	us	10.80	0.53	5.1E-03	10.67	n. d.	C_4AcH_{11}, C_3AH_6

[1]Calculated values assuming equilibrium with monocarboaluminate [2]measured at 25 °C [3]measured at 23 °C. Abbreviations: us — undersaturation, ss — supersaturation.

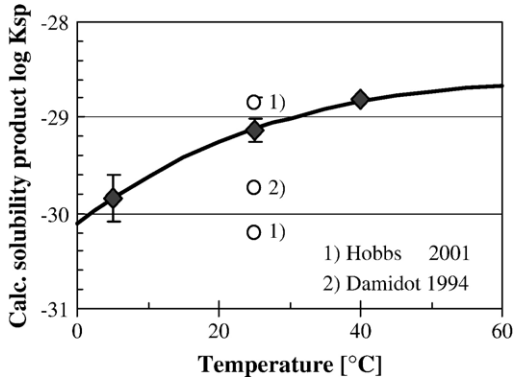

Fig. 16. Calculated solubility products of hemicarboaluminate from solubility experiments (line shows calculated best fit).

increasing proportions of C_3AH_6 and monocarboaluminate develop. It is tentatively concluded that the upper thermal stability limit of hemicarboaluminate is 45±5 °C.

5.2.4. C_4AH_{13}–C_2AH_8, $Ca_4Al_2(OH)_{14}\cdot 6H_2O$–$Ca_2Al_2(OH)_{10}\cdot 3H_2O$

The system $CaO–Al_2O_3–H_2O$ has been much studied at different temperatures generating numerous solubility data. The main datasets at or below ambient temperature are those of D'Ans [35] (20 °C), Wells [17] (21 °C) and Faurie–Mounier [63] (20 °C), Butler [38] (5 °C) and Carlson [39] (1 °C). Depending on the initial bulk Ca/Al ratio, two different hexagonal C–A–H phases were observed: C_2AH_8 was the main C–A–H phase at Ca/Al-ratios ~1 whereas C_4AH_x dominated at high Ca/Al ratios, ≥2.

The solubility data from different literature sources were used to calculate temperature-dependent solubility products of C_4AH_{13}, C_2AH_8 and CAH_{10} (Fig. 19). The data trends are relatively consistent comparing 5 °C and 25 °C. Additional data for C_4AH_{13} obtained in the course of the title study are listed in Table 10.

The stability of C_4AH_x relative to mixtures of portlandite and C_3AH_6 is in dispute. Broadly the literature offers two interpretations; citations [17,35,63] report that C_4AH_x decomposes rapidly to mixtures of C_3AH_6 and portlandite at and above 20–25 °C. On the other hand, Carlson [39], Roberts [40], Seligman and Greening [64] and van Arndt and Visser [65] report the opposite: C_3AH_6 and portlandite react with formation of C_4AH_x, at low temperatures, 1–5 °C.

Furthermore Butler and Taylor [38] and Carlson [39] show the apparent stable formation of CAH_{10} at low Ca/Al ratios and temperatures ≤5 °C. Butler and Taylor report that CAH_{10} is a stable phase in the system $CaO–Al_2O_3–H_2O$ and thus C_2AH_8 should decompose to a mixture of CAH_{10} and C_4AH_{13} at low temperatures. However subsequent investigations by Percival and Taylor [66] have led to the conclusion that CAH_{10} is not stable at temperatures above 21 °C. We return to these discrepancies subsequently.

Only Peppler and Wells [34] gave solubility data for C_4AH_{13} at higher temperatures, >25 °C. Analysis of the phase composition showed increasing amounts of C_3AH_6 formed upon prolonged aging at temperatures ≥50 °C, which indicates decomposition of C_4AH_{13} and C_2AH_8 at elevated temperatures. However the early–age values of C_2AH_8 and C_4AH_{13}, before the onset of significant decomposition, are close to the values reported here. D'Ans [35] observed the same stability trend for prolonged ageing at 25 °C. Hobbs [53] showed significant differences between solubility data obtained from undersaturation (aged ~515 days) and supersaturation (aged ~170 days). Major differences in the aluminium concentration caused large deviations between the solubility products calculated from under- and supersaturation. Nevertheless, relative to the many sources of data, there is generally good agreement between the various solubility datasets. The fitted value of C_4AH_{13} for $\Delta_f H^0$ (−8302 kJ/mol) agrees reasonably with the calculated data by Babushkin et al. [1] ($\Delta_f H^0$ ~−8318 kJ/mol). But $\Delta_f G^0$ of C_4AH_{13} (−7326.6 kJ/mol) is significantly lower than was calculated by Babushkin et al. ($\Delta_f G^0$ ~−7347.8 kJ/mol). The

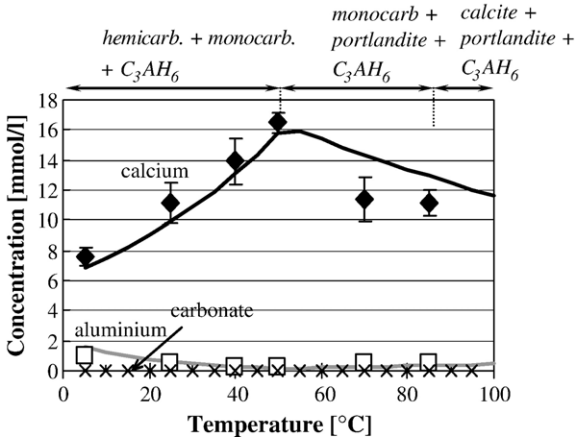

Fig. 17. Recalculated solubility data for nominally hemicarboaluminate based on fitted thermodynamic data from Fig. 16 (markers show experimental values from the title study, lines show calculated fits). Predicted solid phases are shown at the top.

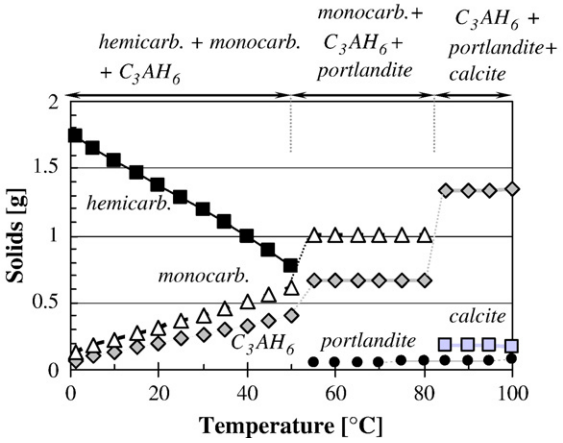

Fig. 18. Calculated mass balance of initially hemicarboaluminate (2 g hemicarboaluminate reacted in 60 g water at selected temperatures between 1–99 °C). Predicted solid phases are shown at the top. Note the discontinuities at ~50 °C and 80 °C, resulting from phase changes (shown at the top).

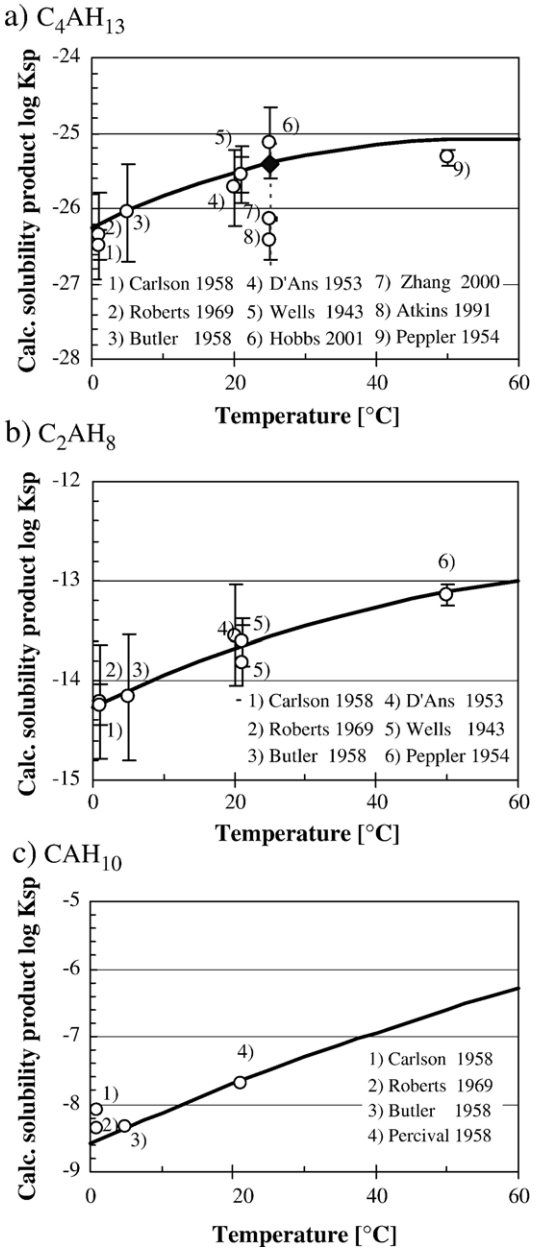

Fig. 19. Calculated solubility products of C_4AH_{13}(a) and C_2AH_8 (b) and CAH_{10} (c) from literature solubility data.

data for C_2AH_8 ($\Delta_f G^0$ ~−4813 kJ/mol, $\Delta_f H^0$ ~−5433 kJ/mol) are in very good agreement with Babushkin et al. ($\Delta_f G^0$ ~−4818 kJ/mol, $\Delta_f H^0$ ~−5436 kJ/mol). The estimated values for CAH_{10} ($\Delta_f G^0$ ~−4622 kJ/mol, $\Delta_f H^0$ ~−5320 kJ/mol) agree very well with the calculated data by Babushkin et al. [1]: ($\Delta_f G^0$ ~−4618 kJ/mol, $\Delta_f H^0$ ~−5320 kJ/mol).

The solubility relations between C_2AH_8, C_4AH_{13} and CAH_{10} are shown in Fig. 20 together with the calculated solubilities of gibbsite and hydrogarnet. With the estimated thermodynamic data, experimental solubility values can be recalculated and are found to agree well with the experimental data. As noted previously, C_4AH_{13} decomposes to a mixture of C_3AH_6 and portlandite with time at 25 °C. Thus the metastability of C_4AH_x phases with respect to C_3AH_6 has to be suppressed to enable recalculation of the solubility values, shown in Fig. 20; the trend lines illustrate the recalculated solubilities of the C–A–H phases using thermodynamic data from the title study. As shown by a dashed line, C_2AH_8 (Fig. 20 (a), curve a–b, is metastable with respect to CAH_{10} and C_4AH_{13} at 5 °C. Metastable and stable aqueous invariant points from Fig. 20 are listed in Table 11; C_4AH_{13} is predicted to decompose to C_3AH_6 and portlandite at 20 °C, but is computed to be stable at 5 °C, indicating an upper limit of thermal stability for C_4AH_{13} at ~10 °C.

5.2.5. Strätlingite, $Ca_2Al_2SiO_2(OH)_{10}\cdot 3H_2O$

The XRD-reflections of the strätlingite preparation (Fig. 21) are broadened and the intensities are relatively weak, indicating poor crystallinity, although the position and relative intensities of all reflections agree with the pattern calculated from structural data by Kuzel [67] and by Rinaldi et al. [68]. According to Kwan et al. [69], who used a method similar to that of the title study to synthesize strätlingite, the reflection at ~29.5° 2θ (CuKα of radiation) may be attributed to C–S–H impurity. Furthermore this reflection overlaps with the main reflections of calcite. In the title study, the peak intensities did not change over the temperature range studied. Thus slight contamination of the samples with respect to calcite cannot be excluded. After several dispersions, a slight decrease of the intensities of the XRD-reflections of strätlingite was observed compared to the fresh sample.

In agreement with Kuzel [67] the thermal analysis pattern of strätlingite (Fig. 22) showed three endothermic peaks (a minor peak at ~120 °C and main peaks at ~165 °C and 220 °C). The total water content of the sample used in the title study, after drying over saturated $CaCl_2$ solution at 37% R.H., is 32.4 wt.%, close to the theoretical value (34.4 wt.% for $Ca_2Al_2SiO_2(OH)_{10}\cdot 3H_2O$) and in good agreement with values obtained on natural strätlingite (32.5 wt.%) by Rinaldi [68]. As C–S–H has a lower percentage water content than strätlingite at 37% R.H. [70], it is believed that at most only a small amount of C–S–H can be present (<10–15%); had more C–S–H been present, the total weight loss of the sample would have been significantly reduced due to dilution by C–S–H. Fig. 22 shows the foil-like morphology of synthetic strätlingite. No distinction between strätlingite and possible contaminants (C–S–H, or calcite, or mixtures thereof) was possible because of their morphological similarities.

Table 10
Solubility data of nominally hydroxy–AFm (C_4AH_{13}) at 25 °C

C_4AH_{13} (from supersaturation)						
Age	Temperature	Ca	Al	pH	Log_K_{sp}	Phases
[Day]	[°C]	[mmol/l]	[mmol/l]			
28	25	17.64	0.21	12.44 (12.40)	−25.60	C_4AH_{13}, C_3AH_6
56	25	20.11	0.20	12.49 (12.46)	−25.21	C_4AH_{13}, C_3AH_6
430	25	19.91	0.17	12.48 (12.43)	(−25.38)	C_3AH_6, $Ca(OH)_2$, C_4AH_{13} traces

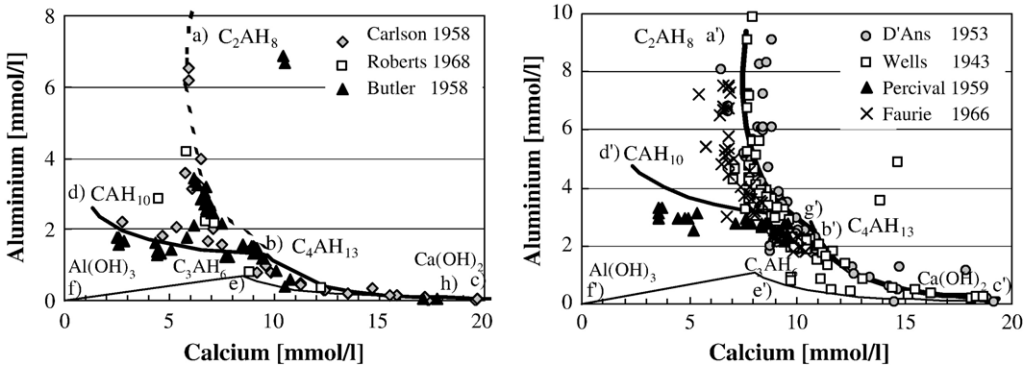

Fig. 20. Solubility relations between C_2AH_8, C_4AH_{13} and CAH_{10} in the system $CaO–Al_2O_3–H2O$ at 5 °C (left) and 25 °C (right) (markers show experimental values, solid lines show calculated results). The relevant aqueous compositions are given in Table 10.

Solubilities of the synthetic strätlingite samples have been obtained in the range from 5 to 85 °C and are listed in Table 12. In one series of experiments, significant amounts of sodium were found to be present in the solution, indicating insufficient washing of the synthesized solids before redispersion. However electron microprobe analysis of the solids did not show significant incorporation of sodium into the structure and data obtained from this preparation were admitted to solubility product calculations; the resulting values are in good agreement with those obtained from preparations known to be sodium-free. The averaged isothermal solubility products, used to estimate the enthalpy of reaction, are given in Fig. 23. It is noteworthy that, although only few solubility data for strätlingite are available, the differences between solubility products calculated from the literature [12,15,71–73] are small; they agree well with our results at 25 °C, even though different procedures had been used to synthesise strätlingite. The resulting thermodynamic data are compiled in Table 2.

In agreement with results by Atkins et al. [12], it was found that the number of redispersions significantly influences the solubility of synthetic strätlingite. Calcium and aluminium concentrations generally decrease with increasing cycles of redispersion, whereas the silicon concentration increases. According to Atkins et al. [12], synthetic strätlingite tends to decompose with increasing redispersions to a C-A-S-H gel the presence of which alters the solubilities significantly. Accordingly, the maximum number of redispersions was limited in the title study to two.

As shown in Fig. 24 and Table 12, experimentally-derived solubilities of calcium and aluminium from strätlingite tend to increase with increasing temperature, whereas the silicon concentrations remain relatively constant. With the help of the fitted thermodynamic data (Table 2), solubility data were also recalculated to assess the impact of residual sodium, assuming an arbitrary aqueous concentration of 2 mmol sodium. Although our solubility measurements agree well with the values by Atkins et al. [12], recalculation did not reproduce the experimental data. A computation of the solubility data in the presence of C–S–H, believed to be present as an impurity, using the solid solution model described by Kulik et al. [30] and by Lothenbach et al. [77], resulted in great differences compared to the experimental values. However if a slight excess of calcium and aluminium (bulk amounts of CaO and Al_2O_3 ~1 wt.% higher than initially admitted to calculation) were artificially added, this was sufficient to reconcile calculation and experiment. Reasons for this behaviour are not clear: the water content of the $Na_2Si_2O_5·2H_2O$ reactant needs to be checked. On the other hand, it is not clear how to treat the contaminants thermodynamically as long as uncertainties remain about their exact amount and composition and further investigations are needed to solve this problem. However the consistency between the literature data and those obtained in the title study should encourage the user to treat these data as useful but not definitive.

Table 11
Calculated chemical composition of aqueous solution at metastable and stable invariant points in the system $CaO–Al_2O_3–H_2O$ at 5 and 25 °C

Temperature [°C]	Point (Fig. 20)	Coexisting solids	Ca [mmol/l]	Al [mmol/l]	pH
Metastable invariant points					
5	b	CAH_{10} and C_4AH_{13}[1]	9.84	1.10	12.93
25	b′	C_2AH_8 and C_4AH_{13}[1]	10.80	2.52	12.19
25	c′	C_4AH_{13} and $Ca(OH)_2$ (portlandite)[2]	19.38	0.18	12.48
25	g′	CAH_{10} and C_2AH_8	9.82	3.03	12.14
Stable invariant points					
5	d	C_3AH_6 and $Al(OH)_3$ (gibbsite)	8.51	0.68	12.88
5	c	C_4AH_{13} and C_3AH_6	18.71	0.07	13.22
5	c	C_4AH_{13} and $Ca(OH)_2$ (portlandite)	21.15	0.04	13.27
25	d′	C_3AH_6 and $Al(OH)_3$ (gibbsite)	8.03	1.09	12.10

[1]Metastable with respect to C_3AH_6 and gibbsite [2]metastable with respect to C_3AH_6 and portlandite.

5.2.6. Monosulfoaluminate–hydroxy–AFm solid solution at 25 °C, $Ca_4Al_2(SO_4)_x(OH)_{14-2x}·6H_2O$

The phase relations between the AFm phases likely to occur in Portland cement were systematically investigated in [62]. AFm phases form only limited mutual solid solutions under conditions likely to obtain in cement environments. It was found that monosulfoaluminate and hydroxy–AFm interact

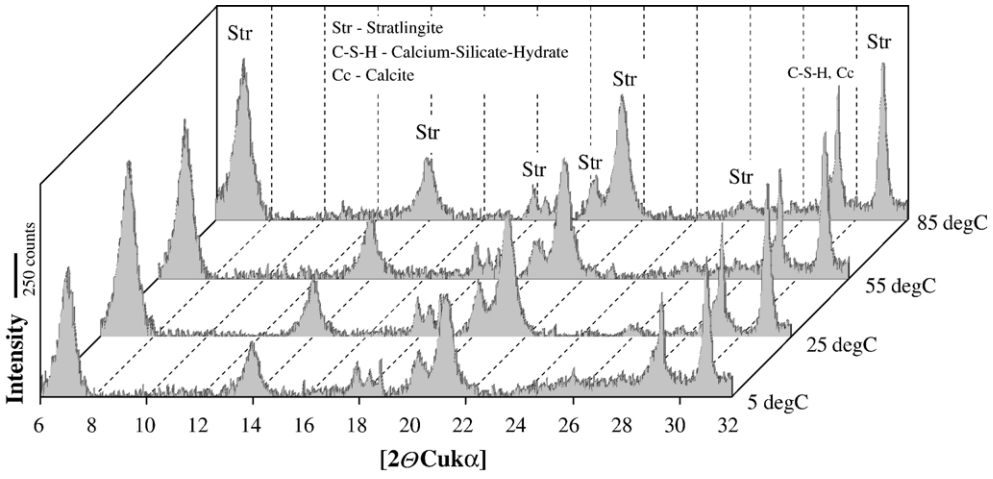

Fig. 21. Comparison of XRD-patterns of nominally strätlingite after ageing at temperatures in the range 5–85 °C (approach from undersaturation).

with each other and form a limited binary solid solution, characterised by sulfate replacing up to ~50% of the hydroxide.

Thus according to our own investigations [62], and in agreement with observations by Poellmann [74] and Roberts [57] ~50 mol% of the initial sulfate in monosulfoaluminate may be replaced by hydroxide due to extensive solid solution formation. According to Poellmann, sulfate substitution is unlikely to occur in the structure of hydroxide–AFm (C_4AH_x). Our investigations showed the presence of a single AFm phase at an initial molar $SO_4/(2OH+SO_4)$ ratio=0.05. This might indicate slight sulfate incorporation into the hydroxy–AFm end member. Nevertheless, it is difficult to interpret the results with precision due to the prevailing detection limits of the XRD method. Thus uncertainties persist about the extent of substitution of sulfate in hydroxide–AFm at the 0–5% replacement level. A detailed description of synthesis and characterisation of the solid solution series is given in [62].

With the aid of the previously derived thermodynamic data of monosulfoaluminate and hydroxy–AFm (Table 2) and the described non-ideal solid solution model, the thermodynamic properties of the solid solution series can be computed. According to the procedure described in Section 4.4, two dimensionless parameters, a_0 and a_1, defined in Eq. (18), were introduced to determine the excess Gibbs energy of mixing. Their numerical values were determined using the software MBSSAS [32] and the known compositional boundaries of the miscibility gap in the solid solution series.

In agreement with experimental data, the miscibility gap fractions of C_4AH_x were set to $0 \le x_1 \le 0.5$ and $0.97 \le x_2 \le 1$ ($x+y=1$), the latter to accept some sulfate substitution in the hydroxy–AFm phase according to Eq. (21):

$$x\left(C_3A \cdot Ca(OH)_2 \cdot nH_2O\right) + y(C_3A \cdot CaSO_4 \cdot nH_2O) \xrightarrow{+H_2O} (x+y)C_3A \cdot \left(Ca(OH)_2\right)_x \cdot (CaSO_4)_y \cdot nH_2O \quad (21)$$

Thus 50% of the initial sulfate in the monosulfoaluminate structure may be replaced by hydroxide and 3% of hydroxide may be replaced by sulfate in the structure of hydroxy–AFm. Assuming this miscibility gap, the dimensionless Guggenheim parameters were estimated to be $a_0=0.188$ and $a_1=2.49$ at 25 °C. Fig. 25 compares the functions of the Gibbs free energy of ideal mixing, ΔG_{id}, the estimated excess Gibbs free energy of mixing ΔG_{ex} and the resulting estimated Gibbs free energy of mixing of the monosulfoaluminate–hydroxide–AFm solid

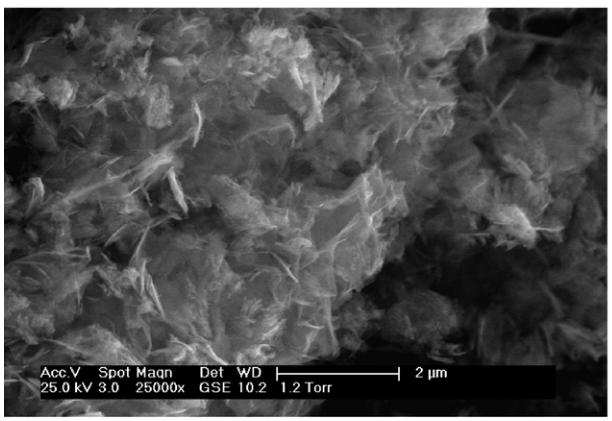

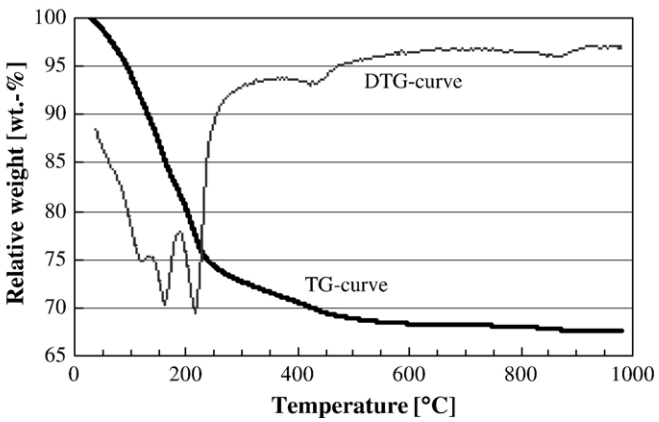

Fig. 22. SEM image of strätlingite (left) and corresponding TG- and DTG curves at 10 °C/min in N_2 (right).

Table 12
Solubility data of strätlingite (C_2ASH_8) at temperatures 5–85 °C

C_2ASH_8 (samples from undersaturation[1])								
Age	Temperature	Ca	Al	Si	Na	pH	Log_K_{sp}	Phases
	[°C]	[mmol/l]	[mmol/l]	[mmol/l]	[mmol/l]			
28	5	1.78	0.47	0.05	<0.2	12.18	−19.89	n.d.
56[1]	5	1.38	0.28	0.06	<0.2	12.08	−20.46	n.d.
84[1]	5	1.44	0.17	0.05	<0.2	12.12	−20.92	C_2ASH_8, C–S–H
28	5	1.68	0.40	0.05	2.35	12.41	−20.08	n.d.
56	5	1.95	0.44	0.04	2.80	12.49	−20.03	n.d.
84[1]	5	1.32	0.31	0.06	0.91	12.20	−20.35	C_2ASH_8, C–S–H, Calcite
28	25	1.75	0.32	0.07	<0.2	11.45(11.58)[2]	−19.82	n.d.
28	25	1.75	0.33	0.07	<0.2	11.45(11.54)[2]	−19.82	n.d.
28	25	1.21	0.35	0.09	<0.2	11.26(11.35)[2]	−20.00	C_2ASH_8, C–S–H
56[1]	25	1.55	0.24	0.09	<0.2	11.40(11.40)[2]	−20.05	n.d.
56[1]	25	1.58	0.24	0.09	<0.2	11.41(11.37)[2]	−20.06	n.d.
56[1]	25	1.75	0.23	0.10	<0.2	11.46(11.42)[2]	−19.95	C_2ASH_8, C–S–H
28	25	1.66	0.50	0.05	2.17	11.65(11.70)[3]	−19.64	n.d.
56	25	1.94	0.45	0.05	2.60	11.73(11.75)[3]	−19.61	n.d.
84[1]	25	1.23	0.33	0.07	0.90	11.41(11.48)[2]	−20.14	C_2ASH_8, C–S–H, Calcite
28	40	2.04	1.00	0.05	2.17	11.21	−18.91	n.d.
56	40	2.03	1.00	0.04	2.60	11.24	−18.99	n.d.
84[1]	40	1.42	0.53	0.08	1.05	11.02	−19.57	C_2ASH_8, C–S–H, Calcite
28	50	1.93	0.50	0.09	<0.2	10.74	−19.23	n.d.
56[1]	50	2.14	0.43	0.11	<0.2	10.79	−19.14	C_2ASH_8, C–S–H
28	50	1.95	0.79	0.05	2.26	10.95	−19.13	n.d.
56	50	1.90	0.76	0.05	2.40	10.95	−19.13	n.d.
84[1]	50	1.49	0.49	0.08	1.14	10.78	−19.53	C_2ASH_8, C–S–H, Calcite
28	70	1.98	1.56	0.04	2.28	10.13	−18.76	n.d.
56	70	2.03	1.60	0.04	2.20	10.14	−18.74	n.d.
84[1]	70	1.77	1.22	0.06	1.50	10.12	−18.87	C_2ASH_8, C–S–H, Calcite
28	85	1.95	1.01	0.07	<0.2	9.89	−18.89	n.d.
56[1]	85	1.80	0.71	0.11	<0.2	9.89	−19.06	n.d.
28	85	2.09	1.50	0.04	2.30	10.13	−18.79	n.d.
56	85	2.07	1.55	0.03	2.30	10.12	−18.87	n.d.
84[1]	85	1.75	1.08	0.07	1.50	10.03	−19.02	C_2ASH_8, C–S–H, Calcite

[1]Solids filtered and redissolved after previous extraction [2]measured values at 23 °C [3)]measured values at 24 °C.

solution series, ΔG_M, according to Eqs. (14–16). The Gibbs energy of the solid solution can be estimated according to Eq. (13) as the sum of the partial Gibbs energies of monosulfoaluminate and hydroxide AFm and ΔG_m, Fig. 25. However, due to uncertainties about the exact upper and lower limit of the miscibility gaps, the derived numerical values should be regarded as provisional, because they are sensitive to changes of the compositional boundaries of the miscibility gap. A more extended discussion about the estimation of the dimensionless Guggenheim parameters in connection with the use of Lippmann phase diagrams is provided in [76].

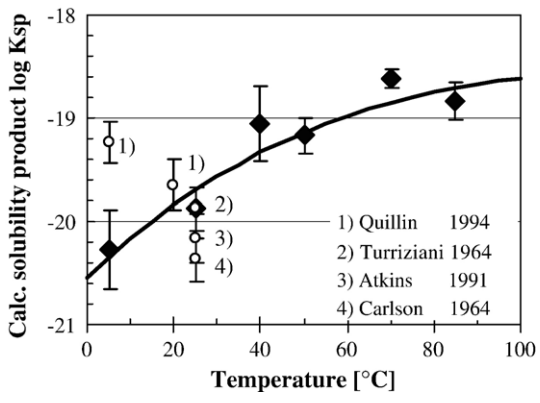

Fig. 23. Calculated solubility products of strätlingite from solubility experiments (line shows calculated best fit).

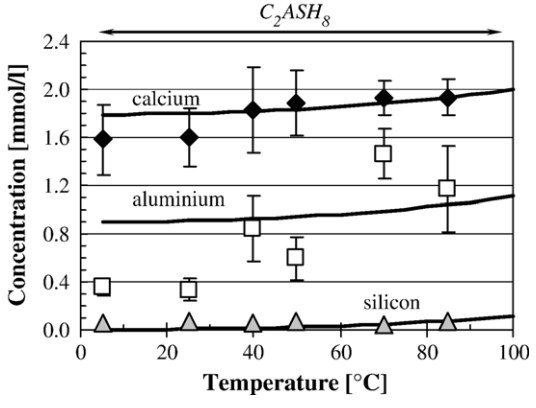

Fig. 24. Recalculated solubility data for strätlingite based on fitted thermodynamic data from Fig. 23 (markers show experimental values from this study, lines show calculated fit). Predicted solid phases are shown at the top.

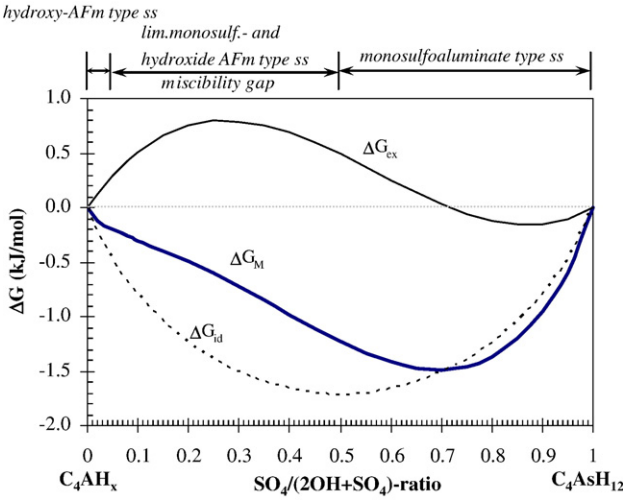

Fig. 25. Gibbs free energy of ideal mixing, ΔG_{id}, excess Gibbs free energy of mixing, ΔG_{ex}, and resulting Gibbs free energy of mixing, ΔG_M, calculated from Eq. (14) for the monosulfoaluminate–hydroxide–AFm solid solution series.

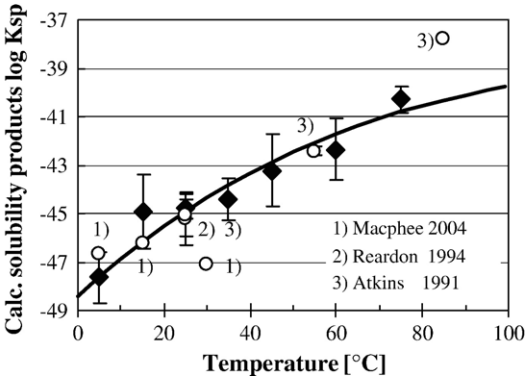

Fig. 27 Calculated solubility products of ettringite according to solubility experiments by Perkins and Palmer [14] (◆) and other literature sources (line shows calculated fit).

Our best fit of the calculated solubilities of the monosulfoaluminate–hydroxy–AFm solid solution series, compared to experimental solubility data at 25 °C, was obtained with the assumed compositional boundaries of the miscibility gap and the resulting Guggenheim parameters (a_0=0.188 and a_1=2.49). As shown in Fig. 26, comparison between experimentally-derived solubility data using averaged values from super- and undersaturation and calculated solubilities of the monosulfoaluminate–hydroxide–AFm solid solution at 25 °C shows excellent agreement in the range $0.05 \le SO_4/(2OH+SO_4) \le 1$, which accounts for the good internal consistency of the dataset. Only the solubility data for the pure hydroxide–AFm end member differ significantly from the calculated values. This behaviour can be explained by the metastability of C_4AH_x with respect to C_3AH_6 and portlandite. As this decomposition reaction of C_4AH_x was only observed in the sulfate-free preparation this might indicate stabilisation of the hydroxy–AFm end member by substitution of small amounts of sulfate in the structure. Fig. 26 b) shows that the aqueous sulfate concentrations are generally very low and at $SO_4/(2OH+SO_4)$ ratios ≤ 0.8 lie below the analytical detection limit. Except for the hydroxy–AFm end member, the predicted phase assemblages agreed well with the experimentally observations. In agreement with XRD analysis, small amounts of AFt were predicted to coprecipitate at $SO_4/(2OH+SO_4)$ ratios ≥ 0.98; also, traces of C_2AH_8 were both predicted and observed at $SO_4/(2OH+SO_4)$ ratios ≤ 0.80 (see [62]).

Poellmann et al. [75] reported recently that monosulfoaluminate–hydroxy–AFm solid solutions may interact with hemicarboaluminate forming limited ternary solid solutions including carbonate, sulfate and hydroxide ions. However no solubility data for these solid solutions are available. Therefore these ternary solid solutions cannot as yet be integrated into the dataset to assess their thermodynamic stability and relations with other hydrate phases.

5.3. AFt-phases

5.3.1. SO_4–AFt, $Ca_6Al_2(SO_4)_3(OH)_{12}\cdot 26H_2O$

Solubility data by Perkins and Palmer [14] for SO_4–AFt were fitted by Lothenbach et al. [77] in the range from 5–75 °C using the software GEMS using the same thermodynamic database as the title study; these data were adopted. Heat capacity coefficients were obtained experimentally from calorimetric heat

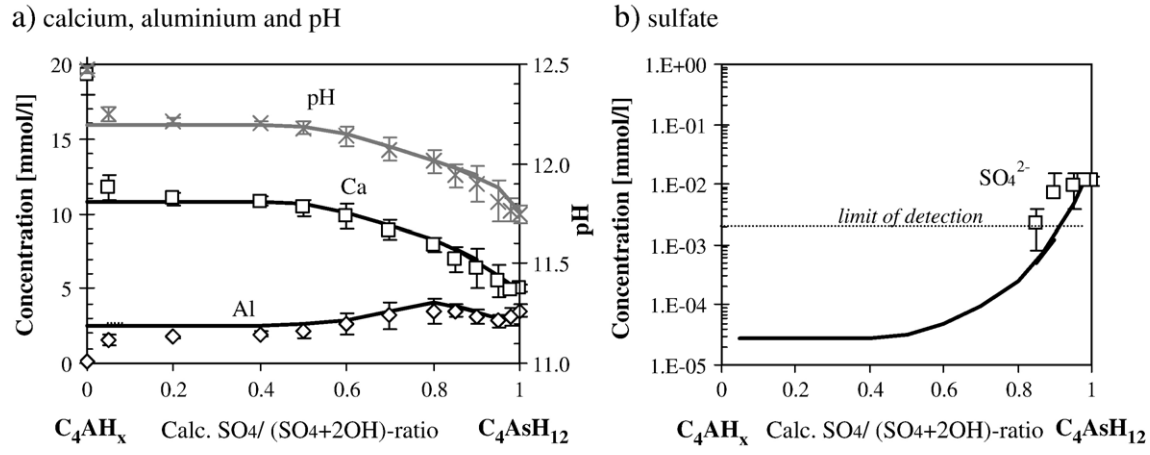

Fig. 26. Solubility data for SO_4–AFm and OH–AFm solid solution series (markers show experimental values from this study, lines show calculated values).

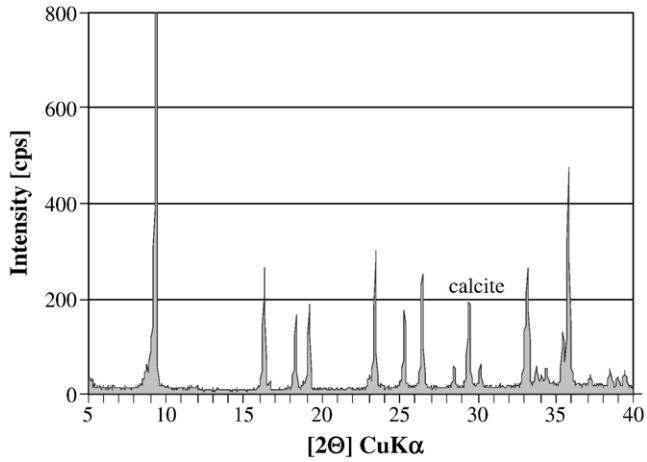

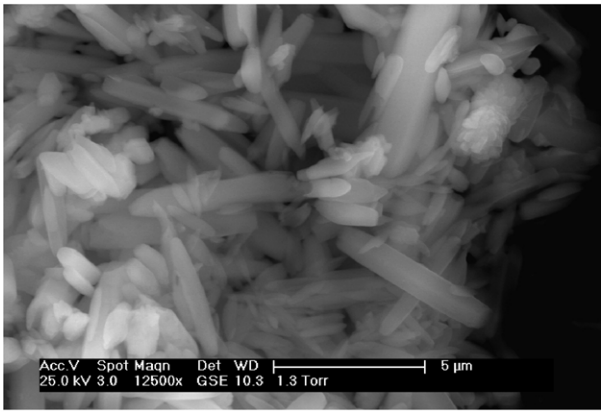

Fig. 28. XRD pattern (left) and scanning electron micrograph (right) of CO_3–AFt used for solubility determinations.

capacities by Ederova [27]: the derived standard molar thermodynamic properties of SO_4–AFt are listed in Table 2.

Fig. 27 shows a comparison of calculated solubility products based on the fitted standard thermodynamic properties of SO_4–AFt with solubility products calculated from experimental solubilities of SO_4–AFt at different temperatures and from different literature sources 12–15,78]. As shown in Fig. 27, the values generally agree within limits of analytical errors: $\Delta_f G^0$ (−15,205.9 kJ/mol) and $\Delta_f H^0$ (−17,535 kJ/mol), consistent with values calculated by Babushkin et al. [1] ($\Delta_f G^0$ ∼ −15,205.7 kJ/mol and $\Delta_f H^0$ ∼−17,578 kJ/mol) and those extrapolated by Perkins et al. [14] ($\Delta_f G^0$ ∼−15,211 kJ/mol and $\Delta_f H^0$ ∼−17,550 kJ/mol). $\Delta_f H^0$ is in reasonable accord with calorimetrically-derived values of Berman [79]: $\Delta_f H^0$ ∼ −17,543 kJ/mol.

5.3.2. CO_3–AFt, $Ca_6Al_2(CO_3)_3(OH)_{12}\cdot 26H_2O$

The existence of a carbonate analogue of SO_4–AFt was first described by Carlson and Berman [16]. However, as shown in [16] and subsequently confirmed by Poellmann et al. [80], synthesis of CO_3–AFt has only been achieved in a solution containing sucrose as well as sodium carbonate. This leads to a strong increase of the solubility of calcium in conjunction with high carbonate concentrations. Other synthesis methods under conditions likely to occur in cementitious system were unsuccessful and gave mixtures of monocarboaluminate and calcite, suggesting that CO_3–AFt is metastable with respect to CO_3–AFm in Portland cement pastes. This contention was later proved by Damidot et al. [54] who published the first thermodynamic data for CO_3–AFt.

Poellmann et al. [80] and Barnett et al. [81] showed that incomplete solid solutions formed between SO_4–AFt and CO_3–AFt. Approximately 60% of the sulfate may be replaced by carbonate. Investigations made in the course of the title study confirmed solid solution formation but with a maximum replacement of ∼50% of the sulfate by carbonate at 25 °C. In contrast to Poellmann et al. [80] and Barnet [81], who used a sucrose method with strongly supersaturated solutions with respect to the AFt solid solutions, we prepared solid solutions by mixing previously synthesized SO_4–AFt and CO_3–AFt in

Table 13
Solubility data of CO_3–AFt at 25 °C

$C_6Ac_3H_{32}$								
Age	Temperature		Ca	Al	CO_3^{2-} [1]	pH[2]	Log_K_{sp}	Phases
[Day]	[°C]		[mmol/l]	[mmol/l]	[mmol/l]			
35	25	us	6.04	3.59	0.007	11.86(11.93)	−46.43	CO_3–AFt, Calcite
70	25	us	6.65	3.94	0.007	11.90(11.83)	−46.10	CO_3–AFt, Calcite
70	25	us	6.16	3.49	0.007	11.88(11.83)	−46.37	CO_3–AFt, Calcite
70	25	us	5.59	3.23	0.007	11.83(11.81)	−46.70	n.d.
70	25	us	5.69	3.21	0.007	11.84(11.78)	−46.64	n.d.
70	25	us	5.81	3.15	0.007	11.86(11.83)	−46.58	n.d.
70	25	us	5.96	3.51	0.007	11.86(11.80)	−46.47	n.d.
270	25	us	5.74	3.82	0.007	11.82(11.96)	−46.59	CO_3–AFt, Calcite
270	25	us	5.49	3.59	0.007	11.80(11.90)	−46.74	CO_3–AFt, Calcite
Recalculated values for the metastable dissolution of CO_3–AFt[3]								
–	25	Calc.	5.90	3.93	0.007	11.82	−46.50	CO_3–AFt, Calcite

[1]Calculated values assuming equilibrium with calcite [2]measured at 25 °C [3]metastability with respect to carboaluminates suppressed. Abbreviation: us — undersaturation.

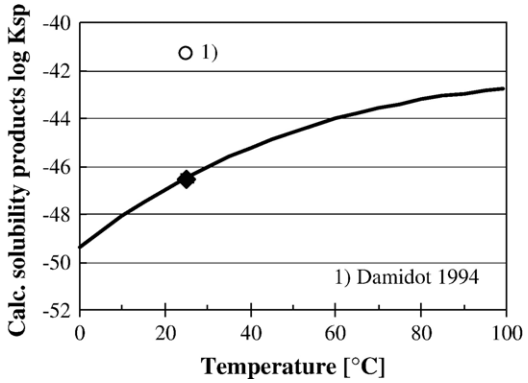

Fig. 29. Calculated solubility product of CO_3–AFt from solubility experiments. The solid diamond shows the single value experimentally determined in the title study. The solid line shows the calculated solubility product: see text and estimated thermodynamic data.

different stoichiometric ratios in ultrapure water at 25 °C (w/s ~30) and aged the mixtures for 6–12 weeks. Afterwards the supernatant and solids were analysed; data confirming extensive and spontaneous AFt solid solution formation are published in [82]. An attempt to model the solid solution behaviour using thermodynamic data for CO_3–AFt given by Damidot et al. [54] failed. A fresh set of solubility experiments was initiated to determine the solubility of CO_3–AFt made using the sucrose method at 25 °C, as described in Section 3.2. Fig. 28 shows the XRD-pattern of the dry CO_3–AFt powder and its typical needle-like morphology. Mixtures of previously dried CO_3–AFt with ultra pure water were aged up to 9 months at 25 °C. Despite the supposed metastability of CO_3–AFt with respect to CO_3–AFm, no obvious mineralogical changes were observed: CO_3–AFt continued to coexist with small amounts of calcite. The solubility data of successive extractions are given in Table 13. The calculated solubility product (log Ksp ~−46.5, $\Delta_f G^0$ ~ −14,565 kJ/mol) differed significantly from the values given by Damidot et al. [54] (log Ksp ~−41.3, $\Delta_f G^0$ ~−14,536 kJ/mol) (see Fig. 29). Hence CO_3–AFt appears to have a lower free energy of formation and is a more stable phase at ≤25 °C than previously concluded. With the new data for CO_3–AFt and SO_4–AFt, together with the non-ideal solid solution model (Section 4.4), it was possible to reproduce the solubility data of the solid solutions with reasonable accuracy (see [82]). The parameters a_0 and a_1, needed to describe the excess Gibbs free energy function, were calculated with the software MBSSAS: the parameters are dependent on the physical location of the compositional boundaries of the miscibility gap. To find an agreement between the slightly differing results reported in the literature compared with our own XRD observations and solubility data, the boundaries of the miscibility gap were set to the mean values $0.04 \le SO_4/(SO_4+CO_3) \le 0.42$. Applying these miscibility limits, the dimensionless Guggenheim parameters of the SO_4–And CO_3–AFt solid solutions were calculated with MBSSAS as $a_0 = -0.823$ and $a_1 = 2.82$. A more extended explanation of the derived parameters, including a discussion of related Lippmann phase diagrams is given in [76].

A thermodynamic sensitivity study [82] showed that major carbonate substitution in SO_4–AFt is unlikely to occur in a "normal" cementitious system at 25 °C, i.e., at carbonate activities conditioned by the presence of an excess of solid $CaCO_3$. In agreement with numerous investigations, monocarboaluminate is thus the energetically favoured carboaluminate phase in calcite-saturated cementitious systems at 25 °C.

Although solubility data for CO_3–AFt have only been determined at 25 °C the temperature-dependent behaviour of CO_3–AFt can be estimated using the Helgeson approach [25]. Data can be approximated for other temperatures by formulating a reference reaction with compounds of similar structure and known entropies. The reference reaction for CO_3–AFt is listed in Table 3. With the known entropies of anhydrite and calcite and the previously estimated value for ettringite (see Table 2) the standard molar entropy of CO_3–AFt was estimated assuming $\Delta S_r^0 = 0$. Subsequently $\Delta_f H^0$ was calculated using the Gibbs-Helmholtz relation (Eq. (12)), the known standard state entropies of the elements [18] and $\Delta_f G^0$. In the literature only one value for $\Delta_f H^0$ was found for CO_3–AFt [1]; ($\Delta_f H^0$ ~−16217 kJ/mol for the 30 H_2O hydrate which equals ~−16789 kJ/mol for the 32 H_2O hydrate) which is in very good agreement with our estimated value ($\Delta_f H^0$ ~ −16792 kJ/mol) for the formula with 32 H_2O. The resulting estimated standard molar thermodynamic data of CO_3–AFt are summarized in Table 2. The computed composition of the aqueous phase in equilibrium with CO_3–AFt and calcite at 25 °C showed good agreement with the averaged solubility data for CO_3–AFt (Table 13).

As noted, although CO_3–AFt is metastable with respect to monocarboaluminate at ~25 °C, free energy plots are a useful instrument to derive data about relative stabilities of phases as a function of temperature. Fig. 30 compares free energy plots for the formation of monocarboaluminate and CO_3–AFt from C_3A and calcite over the temperature range 1 to 99 °C. As expected, monocarboaluminate is thermodynamically more stable than CO_3–AFt between 1 to 99 °C. But with decreasing temperatures CO_3–AFt is increasingly stabilised and is close to being more stable than monocarboaluminate at 1 °C. Due to lack of experimental data and uncertainties in the estimation of thermodynamic properties, the present state of the data must be regarded as provisional. Nevertheless, low temperatures tend to stabilise CO_3–AFt and substitution of SO_4 by CO_3 in the ettringite structure is clearly favoured at low temperatures, <25 °C.

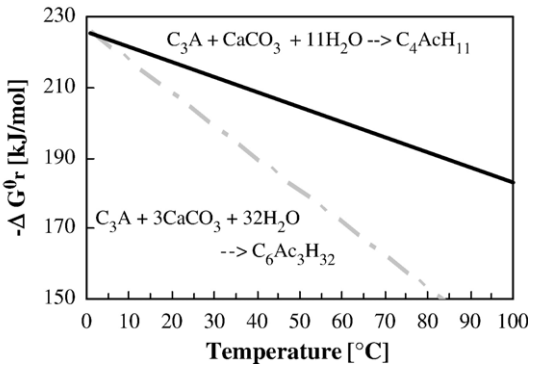

Fig. 30. Free energy plot of the formation of CO_3–AFt and monocarboaluminate from the reaction of C_3A with calcite and water.

Thaumasite is another AFt-type structure containing essential carbonate. In contrast to CO_3–AFt and SO_4–AFt, aluminium is replaced by silicon in thaumasite. According to the literature [83,84], and in contrast to CO_3–AFt, thaumasite has a stability range in the cement system and is preferably formed at low temperatures, <10 °C. This is in agreement with our calculations where we have shown that CO_3-containing AFt structures are stabilised at low temperatures. Furthermore Macphee and Barnett [78] and others [85–87] have shown that SO_4–AFt forms solid solutions with thaumasite. Thus in a real cement system, formation of apparently stable thaumasite-ettringite solid solutions is more likely than the formation of silicon-free (SO_4, CO_3)–AF_t solid solutions even at low temperatures. Macphee and Barnett [78] published solubility data for the solid solutions but not for the thaumasite end member. Bellmann [88] obtained solubility data for natural thaumasite, but only at 8 °C. Thus until recently no complete thermodynamic dataset for thaumasite was available; we are in the course of collating data to (i) predict the temperature-dependent stability of thaumasite and (ii) to enable modelling of the solid solution behaviour between thaumasite and SO_4–AFt.

5.4. C–S–H

C–S–H (calcium–silicate–hydrate) is the main phase of hydrated Portland and blended cements and is responsible for strength development and hydraulic behaviour. Its composition is normally defined by its calcium/silicon ratio. Several authors derived solubilities from synthetic C–S–H [89–96] and the overall picture is consistent. The maximum Ca/Si ratio of C–S–H in hydrated cement pastes is variously claimed to lie between 1.5 and 1.9 in portlandite-saturated systems and, due to phase rule restrictions, C–S–H in Portland cements and blended cements which contain excess portlandite, will have as a first approximation a nearly constant composition ~1.5–1.9$CaO{\cdot}SiO_2{\cdot}nH_2O$, where n is largely dependent on the humidity of the hydrated cement paste. Several thermodynamic models [5,30,97–101] have been developed to describe the solubility properties of C–S–H.

In the title study the ideal solid solution model described in [30] was applied. Tobermorite-type C–S–H (Ca/Si = 0.83), a jennite-type C–S–H (Ca/Si = 1.67) and amorphous silica were used as end members of two different solid solution series, as defined by Lothenbach et al. [77], who gave a detailed description of the derivation of thermodynamic data for the C–S–H end members; we compile these data in Table 2. As shown in Fig. 31, the recalculated solubility of C–S–H agrees reasonably well with literature values.

According to Kulik and Kersten [30] one solid solution (tobermorite–jennite) describes the Ca/Si range $0.83 \le (Ca/Si)_{C-S-H} \le 1.67$ while a second solid solution (amorphous silica–tobermorite) is used to describe the range $0 \le (Ca/Si)_{C-S-H} \le 0.83$. However, according to investigations by Greenberg et al. [92] and Suzuki et al. [94], and as described by Taylor [70], C–S–H gel coexists with a silica species with low calcium content and a composition close to amorphous silica at initial Ca/Si ratios below ~0.6–0.85, indicating either a miscibility gap in the second solid solution series or that it does not have real existence. Therefore the user has to decide which model to apply but, in agreement with the literature, we recommend using a model with *one* solid solution having tobermorite- and jennite-type C–S–H as end members. This allows a coexistence of amorphous silica and C–S–H (Ca/Si = 0.83) at low initial bulk Ca/Si-ratios <0.83, and also enables unambiguous calculation of the range of Ca/Si ratios of most interest to cement paste to be encompassed. These conclusions are supported by recent calculations by Kulik [102].

The C–S–H phase may sorb sulfate, alumina and alkalies. At present, we are not able to include these chemical variants into a thermodynamic model. However, Hong et al. [43] gives distribution coefficients of the sorption of alkalies into C–S–H, which can be used to estimate the amount of sorbed alkalies in C–S–H in dependence of the alkali concentration of the pore solution of the hydrated cement paste. Similarly, the amount of sorbed sulfate can be approximated. Corresponding temperature-dependent values for the adsorption of sulfate to C–S–H are given in [103–106]. Richardson and Groves [106] also describe aluminium for silicon substitution in the C–S–H structure. The amount of substituted aluminium increases with decreasing Ca/Si ratios and can be estimated using the relations described in [106].

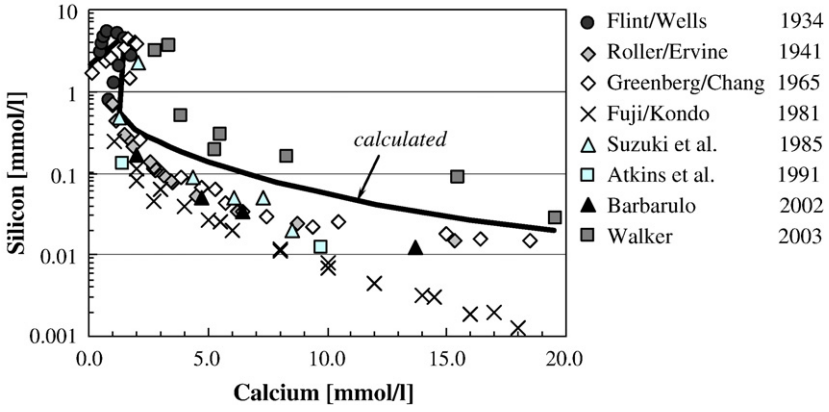

Fig. 31. Comparison of recalculated solubility of C–S–H at 25 °C (solid line) with experimental values from literature (markers) at temperatures between 20–30 °C (see References).

6. Discussion

6.1. Data accuracy

The data for individual substances vary in quality. The reasons for this have been developed in the text but it is still difficult to establish error limits. Firstly, the quality of synthesis is variable: it is difficult if not impossible to establish the absolute phase purity of the preparations. Only the use of single crystals would enable a high confidence in the absolute purity of the preparations used. Secondly, the substances themselves vary in crystallinity with as yet unknown consequences to the numerical values of the data derived from their use. An example is strätlingite, X ray patterns of which always exhibit line broadening associated with low crystallinity, small crystallite size and internal disorder, perhaps with respect to the stacking of successive layers: we have not attempted to deconvolute the causes of line broadening or the impact of crystallinity on thermodynamic properties. But it could be argued that the AFm phase, particularly strätlingite occurring in commercial cements, also exhibits disorder and thus the synthetic is representative of "real" strätlingite.

The results, expressed in tables and diagrams, comprise a working set of data for subsequent calculations. We do not claim that the database is perfect and indeed have noted the shortcomings of particular datasets as appropriate. In a very few cases where data are incomplete, we have also noted work in progress. It is our hope that, as the use of thermodynamic methods become routine, others will add to and improve the accuracy of the compilation.

A general source of experimental uncertainty concerns the analytical data. Some of the very low concentrations, e.g. the aluminium concentrations of C_3AH_6 in equilibrium with portlandite, have numerical values close to the limit of accurate analysis. Carbonate concentrations generally had to be estimated assuming equilibrium with other carbonate phases whose thermodynamic properties were known, e.g., calcite. However, as shown in the title paper, many solubility data generally pass two tests: of self-replication; that is, when used as inputs for calculations they reproduce reliably the input data, usually in the form of solubilities, and second, that they are derived from approach to equilibrium from both oversaturation and undersaturation. This latter test, while not infallible, is generally regarded as substantive proof of the attainment of equilibrium. Moreover the data presented are broadly comparable with those for other substances recorded in the literature. Care was taken to assess all main solubility investigations recorded in the accessible literature. However, as many of the investigations go back to the 1930's, when analytical techniques were often not advanced sufficiently to analyse low concentrations of species, these add another source of uncertainty.

Impurities present in solutions can significantly influence the solubility data. For example a large data scatter was observed for the solubilities of hydrogarnet, C_3AH_6. The older datasets by Wells et al [17] and Peppler et al. [34], used to derive thermodynamic values in previous databases, differ significantly from data obtained in the course of the title study. Wells et al. [17] and Peppler et al [34] used glass flasks in the course of the solubility determinations. Thus it is likely that silicon was dissolved in the course of the experiment. As shown in Section 5.1, silicon can be bound in the hydrogarnet structure and the resulting siliceous hydrogarnet, $Ca_3Al_2(SiO_4)_{3-x}(OH)_{4x}$, will be significantly stabilised and have lower solubility than the silicon-free composition. Atkins et al. [107], who determined solubilities of C_3AH_6 assemblages, confirmed this hypothesis. In the silicon-free samples the solubility product of C_3AH_6 at 25 °C was close to the values obtained in the title study whereas in assemblages containing silicates, e.g. C–S–H and strätlingite, the solubility products attributed to hydrogarnet were significantly lowered. Indeed, Wells and co-workers recognised significant silicon substitution was occurring in the structure of ferrous and aluminous hydrogarnets arising from dissolved silica [108] although no specific statement about the role of silicon impurities was made in their study of "C_3AH_6" solubility.

Furthermore it is generally known that CO_2 interacts strongly with the cement hydrates. Thus, while care was taken in the title study to avoid CO_2-contamination by using in a N_2-atmosphere, traces of carbonate were invariably present.

Another source of uncertainty is the fitting procedure of the experimental data used to derive standard molar thermodynamic data. Kulik [28] gives an overview concerning uncertainties of temperature extrapolations of thermodynamic data. Thermodynamic data of the title study were fitted by a three-term temperature extrapolation and this method is believed to be more reliable than other commonly-used temperature extrapolations [28]. As demonstrated in Fig. 32, solubility products estimated with the widely-used integrated Van't Hoff approach show significantly larger deviations from the experimentally-derived values at elevated temperatures. The difference between extrapolated temperature-dependent solubility products of the hydrates using the three term extrapolation and solubility products, calculated from the fitted standard thermodynamic properties and the estimated heat capacity coefficients according to Section 4.2, are generally small over the temperature range 0 to 99 °C (for example see Fig. 32).

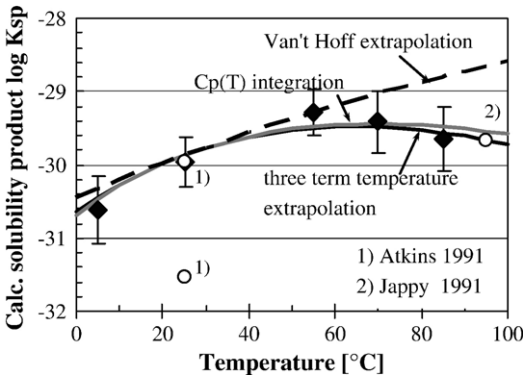

Fig. 32. Comparison of solubility products calculated from the three term temperature extrapolation (solid black line) and integrated Van't Hoff extrapolation (dashed black line) with values calculated using Cp(T) integration (grey line) and experimentally-derived solubility products of siliceous hydrogarnet (markers).

6.2. Relations between equilibrium and kinetics

In the course of preparing this paper we have received numerous comments that, while we study equilibrium, we ignore kinetics. This comment contains an element of truth: it is not possible for us to advance both topics given constraints on resources. But we do not entirely ignore kinetics. For example in the system $CaO–SiO_2–H_2O$, the stable phases tobermorite and jennite are suppressed in favour of metastable C–S–H: C–S–H is assigned a definite set of thermodynamic properties and is allowed to participate in reactions with other phases including some that are thermodynamically stable under the conditions of the calculation. We do this in the knowledge that the C–S–H phase is persistent.

While accepting that the kinetics are important, relatively little progress has been made in their quantification. A thermodynamic approach is immediately successful in showing why this is so. Reactions can be divided into two types: internal, in which overall composition does not change (isochemical) and externally-induced, where cement solids react with their service environment. The latter class of reaction are intrinsically more difficult to quantify because the bulk composition of solids changes in the course of reaction. But thermodynamics immediately shows us that, in seeking to understand the diffusion of a single species into (or out of) cement, it is in fact necessary to constantly recalculate mass balances: diffusion of a single species in isolation is insufficient to account for the overall reactions. A thermodynamic approach, which automatically tabulates mass balances, provides a mass balance template for subsequent kinetic studies and usefully highlights the underlying mechanisms and their probable importance. Many examples are given in the text of reactions which occur relatively rapidly (hours to days) while others occur slowly or not at all. An example of slow reactions is the stability of siliceous hydrogarnet at low temperatures and at low carbonate and sulfate activities (see paragraph below). There also exists a third class of reactions: those predicted to occur but where observation and experiment are inadequate to determine whether or not the relevant prediction is confirmed. It is thus suggested that the kinetics are best approached in conjunction with thermodynamic equilibrium calculations rather than as a separate exercise: the driving forces responsible for change have a thermodynamic basis and, moreover, comparison of calculation and experiment shows that with few exceptions, the principal of local equilibrium is maintained, or nearly so, in the course of environmentally-conditioned reactions.

Many of the verification experiments performed in the course of the title study and in other supporting studies disclose that reaction occurs relatively rapidly: within days or weeks. Of course the experimental conditions were selected to facilitate reaction, as for example, by using high water: solid ratios. Nevertheless further work may disclose that phase changes in cement mineralogy driven by temperature changes occur relatively rapidly. It is of course a well-known generalisation that reaction rates become more rapid at higher temperatures, but perhaps surprisingly, some mineralogical conversion reactions were found to proceed rapidly (days or weeks) at 5 °C. Thus while kinetics are important, much evidence indicates that, with the notable exception of C–S–H, the internal constitution of hydrated Portland cements tends to approach a thermodynamic equilibrium.

6.3. Applications

The database is not in itself a solution to the problems of cement chemistry and mineralogy but, in conjunction with an appropriate computer modelling code, it comprises a tool kit enabling the solution of a broad range of problems. The data presented here have already applied in the calculations presented in references [77,105,109–111] to explore a diverse range of problems including the role of carbonate as a reactive admixture, carbonation of cements and the distribution of sulfate in cement hydration.

Inspection of data tables does not directly reveal relationships between chemistry and mineralogy and its variation with temperature — to see the effects, much thermodynamic modelling calculations are needed. But five features stand out. Firstly, the assemblage of portlandite and C–S–H dominate the products of cement hydration. With few exceptions, these phases persist in most of the assemblages and are rather insensitive in composition to the presence or absence of other phases and, although the C–S–H phase can vary widely in its Ca/Si ratio, its ratio is effectively fixed at or near its highest attainable value (1.5–1.9) by the presence of portlandite. Secondly, the minor phases of hydrated Portland cement (AFm, AFt,...) are very variable in composition and structure. By not forming complete solid solution even within a structural family, the nature of the minor solid remains very sensitive to changes in bulk composition and temperature: note for example, the chemical-mineralogical complexity of the AFm and AFt families. Thirdly the temperature dependence of the nature of the stable phases is quite remarkable and will be explored in a subsequent paper, following additional calculations. Fourthly, changes between assemblages, particularly in respect of the minor phases, require mass transport and structural reconstitution. This creates a series of buffering reactions within the cement paste matrix. For example internal buffering systems exist for hydroxyl, sulfate and carbonate: while the first of these is relatively well-known, the existence of buffers for other species has been less well recognised. The workings of these buffer systems and their interactions, as well as their consequences to environmentally-conditioned reactions of cement systems, will undoubtedly assist the future development of chemical/mineralogical models of cement performance. Finally, the database derived in the title paper redefines the stability of sulfoaluminates hydrates. The undoubted persistence of sulfate AFm amongst the hydration products of commercial cements has long been at variance with its supposed instability at <40 °C: it has been necessary to attribute its persistence to metastability. However, the title study shows sulfoaluminate hydrates to be more stable than hitherto supposed, with a lower limit of thermal stability at ~5 °C in the system $CaO–Al_2O_3–CaSO_4–H_2O$. This revision immediately resolves a long-standing conflict.

Albert et al. [112], have recently suggested that calcium monosulfoaluminate was preserved to lower temperatures, <40 °C, by the reduced activity of water in hydrated cement paste. While they direct attention to an important factor, it is not in fact necessary to invoke special conditions to explain the stability of sulfate AFm according to the revised data. However, we agree with these authors about the importance of extending knowledge of cement hydration to regimes characterised by having reduced water activities, as for example may occur in alkali-activated systems or in normal compositions at low w/s ratios.

The relative thermodynamic stabilities of the cement hydrates are very sensitive to chemical environment. Care has to be taken that the calculated temperature-dependent stability regions for each mineral depend on the total chemical composition of the system and cannot be extrapolated to more complex chemical environments, such as those in commercial cement. Two examples will be discussed briefly:

6.3.1. The influence of sulfate and carbonate on the stability of hydrate phases containing calcium and aluminium

Fig. 33(a) shows the temperature dependent free energy plots of the reaction of tricalcium aluminate (C_3A) and gypsum with water in dependence on the carbonate activity. Until recently it was believed that the assemblage ettringite $+C_3AH_6$ was more stable than monosulfoaluminate [44]. However, applying the dataset of the title study as shown in Fig. 33 (a), for a carbonate-free system with an initial molar bulk ratio $SO_3/Al_2O_3=1$, reactions 2 and 3 show that monosulfoaluminate (C_4AsH_{12}) is calculated to be more stable (Δ_rG^0 of reaction $2<\Delta_rG^0$ of reaction (3)) than a mixture of ettringite (C_6AsH_{32}) and C_3AH_6 at temperatures $>\sim 5$ °C: see Fig. 33. This is in agreement with our own investigations, which have shown that monosulfoaluminate forms and persists at 25 °C for more than 20 months. However the stable hydration products change significantly if carbonate is introduced. According to reaction 1, gypsum will react with part of the alumina to form ettringite whereas the remaining alumina reacts with calcite to form monocarboaluminate. Thus the addition of calcite leads indirectly to a low temperature stabilisation of ettringite in the system.

On the other hand, as shown in Fig. 33 b), monocarboaluminate is predicted to be stable up to 85 °C (reaction (4)) and C_3AH_6 and calcite will be formed at higher temperatures >85 °C, according to reaction (5) (see point *B* Fig. 33 b)). In agreement with the investigations of the title study (see Section 5.2), as well as observations by Kuzel et al. [55], this upper stability temperature (~85 to 90 °C) is valid in the sulfate- free system $CaO–Al_2O_3–CaCO_3–H_2O$. However from these investigations one cannot conclude that monocarboaluminate will be stable up to 85 °C in a sulfate-containing environment, e.g. in Portland cement. In a sulfate-containing system, monocarboaluminate will only be stable up to 50 °C and monosulfoaluminate will instead form according to reaction (2) at higher temperatures; see Point A of Fig. 33 a). This means that the reported upper stability temperature of monocarboaluminate will decrease significantly in hydrated Portland cement where sulfate is normally present.

Several other aspects of the data will require to be investigated. Arguably, the most important concerns the potential for phase changes in cement pastes at low temperatures. Low temperatures, in the range 0°–20 °C, increasingly stabilise carbonate substitution into the ettringite phase.

This potential substitution could enable formation of ettringite without need for additional sulfate and may help explain why enhanced ettringite formation appears to be a precursor to thaumasite: reaction proceeds in two stages by replacement of sulfate in ettringite by carbonate followed by silicate replacement of aluminate, with conversion of carbonate ettringite to thaumasite.

6.3.2. The influence of silica on the stability of hydrate phases containing calcium and aluminium

Silica is one of the main constituents of Portland cements. Fig. 34(a) shows free energy plots of the reaction of C_3A, with gypsum and water. As pointed out previously in the silica-free system $CaO–Al_2O_3–CaSO_4–H_2O$, with an initial molar bulk SO_3/Al_2O_3-ratio=1, monosulfoaluminate is more stable than the phase assemblage of ettringite (C_6AsH_{32}) and C_3AH_6 at temperatures $>\sim 5$ °C (reactions 2 and 3, Fig. 34 (a). But if silicon is added to the system, according to reaction (1) the phase

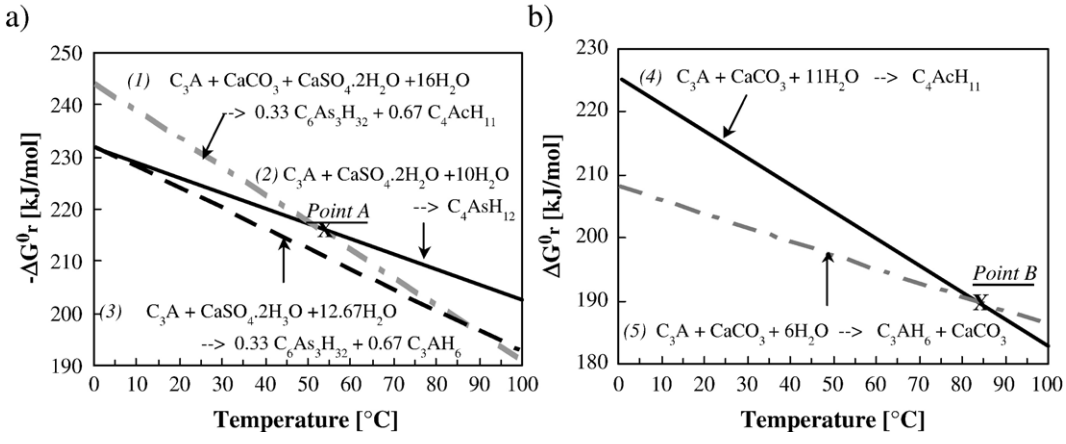

Fig. 33. Influence of sulfate and carbonate on the relative stabilities of aluminate hydrates.

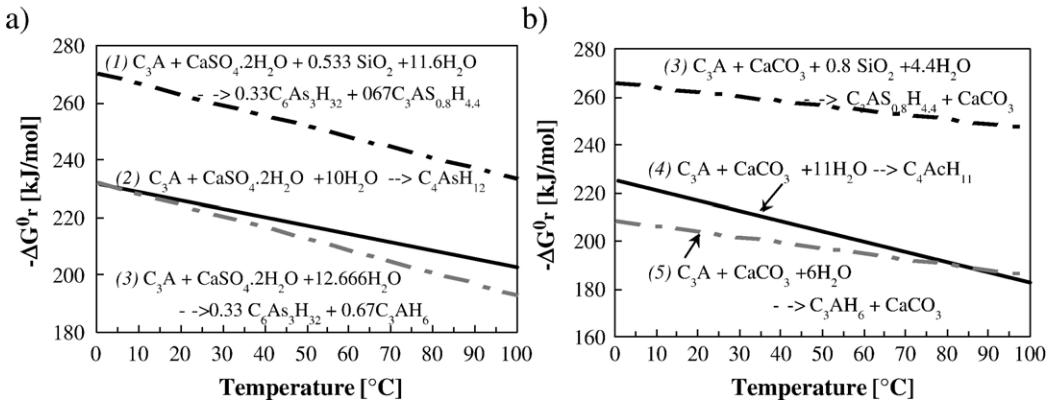

Fig. 34. Influence of silicon on the relative stabilities of aluminate hydrates.

assemblage of C_6AsH_{32} and $C_3AS_{0.8}H_{4.4}$, which represent a member of the solid solution series $Ca_3Al_2(SiO_4)_{3-x}(OH)_{4x}$, has a lower Gibbs free energy of reaction and is therefore thermodynamically more stable than monosulfoaluminate (reaction (2)) at temperatures from 1 to 99 °C. In the system $CaO–Al_2O_3–CaCO_3–H_2O$, addition of silicon causes an analogous thermodynamic stabilisation of the hydrogarnet phase (Fig. 34 b). Whereas in the silicon-free system, monocarboaluminate is calculated to be more stable than the assemblage of C_3AH_6 and calcite at temperatures below ~85 °C, if silica is added according to reaction (4), $C_3AS_{0.8}H_{4.4}$ and calcite becomes more stable than monocarboaluminate. Thus calcite is predicted to be an essentially inert material in the system $CaO–Al_2O_3–CaCO_3–SiO_2–H_2O$ at all temperatures, 1–99 °C.

Probably due to kinetic reasons, siliceous hydrogarnet is rarely observed in hydrated Portland cement at room temperature. Numerous researchers have shown that AFm-phases are abundant reaction products of Portland cements. In agreement with experimental results, sulfate and carbonate AFm-phases are observed as persistent phases in Portland cement.

It is not possible to extrapolate stability regions obtained from simplified model systems with two or three components directly to complex chemical systems, e.g. to commercial Portland cement, with numerous components present. However, with the knowledge of the thermodynamic properties of all potential reaction products and a suitable software, it is possible to undertake the additional calculations necessary to predict and quantify the phase assemblages. On the other hand, as shown above, the database cannot be used as a "black-box" approach and fundamental knowledge about the processes of cement hydration, including the knowledge of reaction pathways and metastable vs. stable phase assemblages–the latter based on experimental observations–is necessary to guide calculations.

Nomenclature in cement chemistry

C	CaO
A	Al_2O_3
S	SiO_2
s	SO_3
c	CO_2
H	H_2O

Other abbreviations used in calculations

A	Debye–Hűckel solvent parameters dependent on the dielectric constant of water and temperature (A = 0.5114 at 25 °C)
α_i	parameter dependent on the size of species, i, taken from Kielland's table (cited in [24])
B	Debye-Hűckel solvent parameters dependent on the dielectric constant of water and temperature (B = 0.3288 at 25 °C)
b_i	common extended Debye–Hűckel parameter (b_i ~ 0.064 at 25 °C)
C_p^0	standard molar heat capacity of species at T, P (J K^{-1} mol^{-1})
$\Delta_r Cp_T^0$	standard molar heat capacity change of reaction at T (J K^{-1} mol^{-1})
$\Delta_r Cp_{T0}^0$	standard molar heat capacity change of reaction at T_0 = 298 K (25 °C) (J K^{-1} mol^{-1})
$\Delta_f G_{T0}^0$	standard molar Gibbs energy (of formation from elements) at T_0 = 298 K (25 °C) (kJ mol^{-1})
$\Delta_r G_T^0$	standard Gibbs energy change in a reaction (kJ mol^{-1})
ΔG_{ex}	excess molar Gibbs energy of mixing for the solid solution series (kJ mol^{-1})
$\Delta_f G_i^0$	standard molar Gibbs energy of formation of end member i of a solid solution series (kJ mol^{-1})
ΔG_{id}	molar Gibbs energy of mixing of an ideal solid solution (kJ mol^{-1})
ΔG_M	molar Gibbs energy of mixing for end members i of the solid solution series (kJ mol^{-1})
ΔG_{ss}	molar Gibbs energy of a solution between different end members i (kJ mol^{-1})
γ_i	Activity coefficient of species i
$\Delta_r H_T^0$	standard change of enthalpy of reaction at T (kJ K^{-1} mol^{-1})
$\Delta_r H_{T0}^0$	standard change of enthalpy of reaction at T_0 = 298 K (25 °C) (kJ K^{-1} mol^{-1})
$\Delta_f H_{T0}^0$	standard molar enthalpy at T_0 = 298 K (25 °C) (kJ K^{-1} mol^{-1})
I	effective molal ionic strength of aqueous solution
K_T	thermodynamic equilibrium constant of reaction at T
R	universal gas constant (8.31451 J K^{-1} mol^{-1})
$\Delta_r S_T^0$	standard entropy change in reaction at T (J K^{-1} mol^{-1})

$\Delta_r S^0_{T0}$ standard entropy change in reaction at T_0=298 K (25 °C) (J K^{-1} mol^{-1})
S^0_{T0} standard molar absolute entropy at T_0=298 K (25 °C) (J K^{-1} mol^{-1})
T temperature of interest (K)
T_0 reference temperature (298 K)
V^0 standard molar volume (cm^3 mol^{-1})
X_i mole fraction of end member i in solid solution

Acknowledgement

The support of NANOCEM, a consortium of European cement producers and academic institutions is acknowledged. The project advisors Ellis Gartner, Lafarge Cement France, Duncan Herfort, Aalborg Cement Denmark and Karen Scrivener, EPFL Lausanne, have contributed to and encouraged our approach. Finally, the manuscript was critically reviewed by Dimitrii Kulik, PSI Switzerland, who gave valuable advise to the use of GEMS-PSI in the course of this project and John Gisby, NPL UK. Their constructive comments have contributed greatly to the published version.

References

[1] V.I. Babushkin, G.M. Matveev, O.P. Mčedlov-Petrosjan, Thermodinamika Silikatov, Strojisdat, Moskau, 1965 (in Russian).
[2] M. Atkins, D.G. Bennet, A.C. Dawes, F.P. Glasser, A. Kindness, D. Read, A thermodynamic model for blended cements, Cement and Concrete Research 22 (1992) 497–502.
[3] D.G. Bennet, D. Read, M. Atkins, F.P. Glasser, A thermodynamic model for blended cements II: Cement hydrate phases; thermodynamic values and modelling studies, Journal of Nuclear Materials 190 (1992) 315–325.
[4] D. Damidot, S.J. Barnett, F.P. Glasser, D. Macphee, Investigation of the $CaO–Al_2O_3–SiO_2–CaSO_4–CaCO_3–H_2O$ system at 25 °C by thermodynamic calculations, Advances in Cement Research 16 (2004) 69–76.
[5] E.J. Reardon, An ion interaction model for the determination of chemical equilibria in cement/water systems, Cement and Concrete Research, vol. 20, 1990, pp. 175–192, S.
[6] E.J. Reardon, Problems and approaches to the prediction of the chemical composition in cement/water systems, Waste Management 12 (1992) 221–239.
[7] B. Lothenbach, F. Winnefeld, Thermodynamic modelling of the hydration of Portland cement, Cement and Concrete Research 36 (2006) 209–226.
[8] L. Clodic, A. Meike, Thermodynamics of calcium silicate hydrates, Development of a Database to Model Concrete Dissolution at 25 °C Using the EQ3/6 Geochemical Modeling Code, Lawrence Livermore National Laboratory, 1997.
[9] X. Bourbon, Chemical conceptual models for cement based materials. Mineral phases and thermodynamic data, Andra Technical Report C.NT. ASCM.03.026., 2003.
[10] R. Ramachandran, P.K. Gupta, An improved spectrophotometric determination of silicate in water based on molybdenum blue, Analytica Chimica Acta 172 (1985) 86–89.
[11] T.G. Jappy, F.P. Glasser, Synthesis and stability of silica-substituted hydrogarnet $Ca_3Al_2Si_{3-x}O_{12-4x}(OH)_{4x}$, Advances in Cement Research 4 (1991/92) 1–8.
[12] M. Atkins, F.P. Glasser, A. Kindness, D.E. Macphee, Solubility data for cement hydrate phases (25 °C), DOE Report No.: DoE/HMIP/RR/91/032, University of Aberdeen, 1991.
[13] C.J. Warren, E.J. Reardon, The solubility of ettringite at 25 °C, Cement and Concrete Research 24 (1994) 1515–1524.
[14] R.B. Perkins, C.D. Palmer, Solubility of ettringite $(Ca_6[Al(OH)_6]_2(SO_4)_3\times26H_2O)$ at 5–75 °C, Geochimica et Cosmochimica Acta 63 (1999) 1969–1980.
[15] M. Atkins, F.P. Glasser, T.G. Jappy, A. Kindness, L.P. Moroni, M. Constable, A. Fenton, D.J. Lee, D.V.C. Jones, A. Cook, C.R. Wilding, Effect of elevated temperature on blended cement in radioactive waste disposal, UK DoE Report, University of Aberdeen, 1991.
[16] E.T. Carlson, H.A. Berman, Some observations on the calcium aluminate carbonate hydrates, Journal of Research of the National Bureau of Standards 64 (1960) 333–341.
[17] L.S. Wells, W.F. Clarke, H.F. McMurdie, Study of the system $CaO–Al_2O_3–H_2O$ at temperatures of 21° and 90 °C, Journal of Research of the National Bureau of Standards (1943) 367–407.
[18] D. Kulik, U. Berner, E. Curti, Modelling chemical equilibrium partitioning with the GEMS-PSI code, PSI Scientific Report IV (2003) 109–122 (http://les.web.psi.ch/Software/GEMS-PSI/).
[19] W. Hummel, U. Berner, E. Curti, F.J. Pearson, T. Thoenen, Nagra/PSI Chemical Thermodynamic Data Base 01/01, Universal Publishers, Parkland, Florida, USA, 2002.
[20] J.W. Johnson, E.H. Oelkers, H.C. Helgeson, SUPCRT92: a software package for calculating the standard molal thermodynamic properties of minerals, gases, aqueous species, and reactions from 1 to 5000 bar and 0 to 1000 °C, Computers & Geosciences 18 (1992) 899–947 (slop98.dat database available from http://affinity.berkeley.edu).
[21] E.L. Shock, D.C. Sassani, M. Willis, D. Sverjensky, Inorganic species in geologic fluids: Correlations among standard molal thermodynamic properties of aqueous ions and hydroxide complexes, Geochimica et Cosmochimica Acta 61 (1997) 907–950.
[22] D. Sverjensky, E.L. Shock, H.C. Helgeson, Prediction of the thermodynamic properties of aqueous metal complexes to 1000 °C and 5 kbar, Geochimica et Cosmochimica Acta 61 (1997) 1359–1412.
[23] T. Thoenen, D. Kulik, Nagra/PSI Chemical Thermodynamic Data Base 01/01 for the GEM-Selektor (V.2-PSI) Geochemical Modeling Code: Release 28-02-03. *PSI Technical Report TM-44-03-04 (unpublished)* about the GEMS version of Nagra/PSI chemical thermodynamic database 01/01. 2003. http://les.web.psi.ch/Software/GEMS-PSI/doc/pdf/TM-44-03-04-web.pdf.
[24] D.K. Nordstrom, J.L. Munoz, Geochemical Thermodynamics, 2nd edition. Blackwell Scientific, Palo Alto, 1994.
[25] H.C. Helgeson, J.M. Delany, H.W. Nesbitt, D.K. Bird, Summary and critique of the thermodynamic properties of rock-forming minerals, American Journal of Science 278–A (1978) 229 pp.
[26] Y. Gu, C.H. Gammons, M.S. Bloom, A one-term extrapolation method for estimating equilibrium constants of aqueous reactions at elevated temperatures, Geochimica et Cosmochimica Acta 58 (1994) 3545–3560.
[27] J. Ederova, V. Satava, Heat capacities of C_3AH_6, C_4ASH_{12} and $C_6AS_3H_{32}$, Thermochimica Acta 31 (1979) 126–128.
[28] D. Kulik, Minimising uncertainty induced by temperature extrapolations of thermodynamic data: a pragmatic view on the intergration of thermodynamic databases into geochemical computer codes, Proceedings the use of thermodynamic databases in performance assessment, Barcelona, OECD, 2002, pp. 125–137.
[29] D. Kulik, Thermodynamic properties of surface species at the mineral–water interface under hydrothermal conditions: a Gibbs energy minimization single-site $2pK_A$ triple-layer model of rutile in NaCl electrolyte to 250 °C, Geochimica et Cosmochimica Acta 64 (2000) 3161–3169.
[30] D.A. Kulik, M. Kersten, Aqueous solubility diagrams for cementitious waste stabilization systems: II, End-member stoichiometries of ideal calcium silicate hydrate solid solutions, Journal of the American Ceramic Society 84 (2001) 3017–3026.
[31] D.A. Kulik, Dual-thermodynamic estimation of stoichiometry and stability of solid solution end members in aqueous-solid solution systems, Geochemical Geology 225 (2006) 189–212.
[32] P.D. Glynn, MBSSAS: a code for the computing of margules parameters and equilibrium relations in binary solid-solutions aqueous-solution systems, Computers & Geoscience 17 (1991) 907–966.

[33] M. Kersten, Aqueous solubility diagrams for cementitious waste stabilization systems: I, The C–S–H solid solution system, Environmental Science & Technology 30 (1996) 2286–2293.
[34] R.B. Peppler, L.S. Wells, The system of lime, alumina, and water from 50° to 250 °C, Journal of Research of the National Bureau of Standards 52 (1954) 75–92.
[35] J. D'Ans, H. Eick, Das System $CaO–Al_2O_3–H_2O$ bei 20 °C und das Erhärten der Tonerdezemente, Zement-Kalk-Gips 6 (1953) 197–210.
[36] J. D'Ans, H. Eick, Das System $CaO–Al_2O_3–CaSO_4–H_2O$ bei 20 °C, Zement-Kalk-Gips 9 (1953) 302–311.
[37] R. Nacken, R. Mosebach, Untersuchungen am System $CaO–Al_2O_3–H_2O$, Zeitschrift fur Anorganische und Allgemeine Chemie Bd. 225 (1934) 289–301.
[38] F.G. Butler, H.F.W. Taylor, The system $CaO–Al_2O_3–H_2O$ at 5 °C, Journal of the Chemical Society (1958) 2103–2110.
[39] E.T. Carlson, The system lime–Alumina–water at 1 °C, Journal of Research of the National Bureau of Standards 61 (1958) 1–11.
[40] M.H. Roberts, Written discussion, in: H.E. Schwiete, U. Ludwig (Eds.), Crystal structures and properties of cement hydration products (hydrated calcium aluminates and ferrites), Proceedings of the V. Intern. Symposium on the chemistry of Cements, Tokyo, vol. II, 1969, pp. 67–71.
[41] H.A. Berman, E.S. Newman, Heat of formation of calcium aluminate monocarbonate at 25 °C, Journal of Research of the National Bureau of Standards. A, Physics and Chemistry 65 (1961) 197–207.
[42] M. Schoenitz, A. Navrotsky, Enthalpy of formation of katoite $Ca_3Al_2[(OH)_4]_3$: energetics of the hydrogarnet substitution, American Mineralogist 84 (1999) 389–391.
[43] S.Y. Hong, F.P. Glasser, Alkali binding in cement paste, Cement and Concrete Research 29 (1999) 1893–1903.
[44] D. Damidot, F.P. Glasser, Thermodynamic investigation of the $CaO–Al_2O_3–CaSO_4–H_2O$-system at 25 °C and the influence of Na_2O, Cement and Concrete Research 23 (1993) 221–238.
[45] F.E. Jones, The quaternary system $CaO–Al_2O_3–CaSO_4–H_2O$ at 25 °C, Journal of Physical Chemistry 48 (1944) 311–350.
[46] G.L. Kalousek, Sulfoaluminates of calcium as stable and metastable phases and a study of a portion of the five-component system $CaO–SO_3–Al_2O_3–Na_2O–H_2O$ at 25 °C. PhD-Thesis, University of Maryland, 1941.
[47] F. Zhang, Z. Zhou, Z. Lou, Solubility product and stability of ettringite, Proceedings of the 7th Intern. Congress on the Chemistry of Cements, vol. II, 1980, pp. 88–93.
[48] M. Zhang, Incorporation of Oxyanionic B, Cr, Mo and Se into hydrocalumite and ettringite: Application to cementitious system. PhD-Thesis, University of Waterloo, Canada, 2000.
[49] H.A. Berman, E.S. Newman, Heat of formation of calcium aluminate monosulfate at 25 °C, Journal of Research of the National Bureau of Standards. A, Physics and Chemistry 67A (1963) 1–13.
[50] D. Damidot, F.P. Glasser, Thermodynamic investigation of the $CaO–Al_2O_3–CaSO_4–H_2O$-system at 50 °C and 85 °C, Cement and Concrete Research 22 (1992) 1179–1191.
[51] V. Satava, Determination of standard enthalpies and Gibbs energies of formation for $6CaO×Al_2O_3×3SO_3×32H_2O$ ($C_6AS_3H_{32}$) and $4CaO×Al_2O_3×SO_3×32H_2O$ (C_4ASH_{12}) by the DHA-method, Silikaty 30 (1986) 1–8.
[52] T. Nishikawa, K. Sato, S. Ito, K. Suzuki, Thermal and chemical stability of AFm-phase-isostructural group, Proceedings of the 9th Intern. Congress on the Chemistry of Cements, vol. I, 1992, pp. 437–442.
[53] M. Hobbs, Solubilities and ion exchange properties of solid solutions between the OH, Cl and CO_3 end members of the monocalcium aluminate hydrates. PhD-Thesis, University of Waterloo, Canada, 2001.
[54] D. Damidot, S. Stronach, A. Kindness, M. Atkins, F.P. Glasser, Thermodynamic investigation of the $CaO–Al_2O_3–CaCO_3–H_2O$ closed system at 25 °C and the influence of Na_2O, Cement and Concrete Research 24 (1994) 563–572.
[55] H.J. Kuzel, H. Baier, Hydration of calcium aluminate cements in the presence of calcium carbonate, European Journal of Mineralogy 8 (1996) 129–141.
[56] P. Seligmann, N.R. Greening, Phase equilibria of cement-water, Proceedings of the V. Intern. Symposium on the Chemistry of Cements, Tokyo, vol. II, 1969, pp. 179–200.
[57] M.H. Roberts, Calcium aluminate hydrates and related basic salt solid solutions, Proceedings of the V. Intern. Symposium on the Chemistry of Cements, Tokyo, vol. II, 1969, pp. 104–117.
[58] F.P. Glasser, A. Kindness, S.A. Stronach, Stability and solubility relationships in AFm phases Part I: Chloride, sulfate and hydroxide, Cement and Concrete Research 29 (1999) 861–866.
[59] H.J. Kuzel, H. Poellmann, Hydration of C_3A in the presence of $Ca(OH)_2$, $CaSO_4×2H_2O$ and $CaCO_3$, Cement and Concrete Research 21 (1991) 885–895.
[60] H.J. Kuzel, Initial hydration reactions and mechanisms of delayed ettringite formation in Portland cement, Cement and Concrete Research 26 (1996) 195–203.
[61] T. Matschei, B. Lothenbach, F.P. Glasser, The role of calcium carbonate in cement hydration, Cement and Concrete Research 37 (2007) 551–558.
[62] T. Matschei, B. Lothenbach, F.P. Glasser, The AFm-phase in Portland cement, Cement and Concrete Research 37 (2007) 118–130.
[63] M.T. Faurie-Mounier, Contribution à l'étude du système $Ca–Al_2O_3–H_2O$, Revue des Matériaux de Construction, 1966, pp. 635–636.
[64] P. Seligmann, R. Greening, New techniques for temperature and humidity control in X-ray diffractometry, Journal of the PCA Research and Development Laboratories 4 (1962) 2–9.
[65] J.H.P. Aarndt van, S. Viesser, Some reactions of tricalciumaluminate hexahydrate at medium temperatures, Cement and Lime Manufacture 40 (1967) 7–11.
[66] A. Percival, H.F.W. Taylor, Monocalcium aluminate hydrate in the system $CaO–Al_2O_3–H_2O$ at 21 °C, Journal of the Chemical Society 526 (1959) 2629–2631 (notes).
[67] H.J. Kuzel, Crystallographic data and thermal decomposition of synthetic gehlenite hydrate $2CaO×Al_2O_3×SiO_2×8H_2O$, Neues Jahrbuch fuer Mineralogie Monatshefte, 1976, pp. 319–325.
[68] R. Rinaldi, M. Sacerdoti, E. Passaglia, Strätlingite: crystal structure, chemistry, and a reexamination, of its polytype vertumnite, European Journal of Mineralogy 2 (1990) 841–849.
[69] S. Kwan, J. LaRosa, M.W. Grutzeck, ^{29}Si and ^{27}Al MASNMR study of Strätlingite, Journal of the American Ceramic Society 78 (1995) 1921–1926.
[70] H.F.W. Taylor, Cement Chemistry, 2nd Edition. Thomas Telford Publishing, London, 1997.
[71] R. Turriziani, The calcium aluminate hydrates and related compounds. Cited in Taylor, H.F.W.: Cement Chemistry, Volume I, p. 233 Academic press, London and New York, 1964.
[72] E.T. Carlson, Written discussion, in: K.T. Greene (Ed.), Early hydration reactions of Portland cement, Proceedings of the IV. Intern. Symposium on the chemistry of Cements, Washington, D.C, vol. IV, 1964, pp. 375–376.
[73] K.C. Quillin, A.J. Majumdar, Phase equilibria in the $CaO–Al_2O_3–SiO_2–H_2O$ system at 5 °C, 20 °C and 38 °C, Advances in Cement Research 6 (1994) 47–56.
[74] H. Poellmann, Solid solution in the system $3CaO×Al_2O_3×CaSO_4×aq–3CaO×Al_2O_3×Ca(OH)_2×aq$, Neues Jahrbuch fuer Mineralogie Abhandlungen 161 (1989) 27–41.
[75] H. Poellmann, Syntheses, properties and solid solution of ternary lamellar calcium aluminate hydroxy salts (AFm-phases) containing SO_4^{2-}, CO_3^{2-} and OH^-, Neues Jahrbuch fuer Mineralogie Abhandlungen 182/2 (2006) 173–181.
[76] Matschei, T., PhD thesis University of Aberdeen, in preparation, 2007.
[77] B. Lothenbach, T. Matschei, G. Mőschner, F.P. Glasser, Thermodynamic modelling of the effect of temperature on the hydration and porosity of Portland cement, Cement and Concrete Research, submitted for publication.
[78] D. Macphee, S. Barnett, Solution properties of solids in the ettringite–thaumasite solid solution series, Cement and Concrete Research 34 (2004) 1591–1598.
[79] H.A. Berman, E.S. Newman, Heat of formation of tricalciumsulfoaluminate at 25 °C, Proceedings of the IV. Intern. Symposium on the chemistry of Cements, Washington, D.C, 1964, pp. 247–257.

[80] H. Poellmann, H.J. Kuzel, R. Wenda, Solid solution of ettringites part I: incorporation of OH^- and CO_3^{2-} in $3CaO{\cdot}A1_2O_3{\cdot}32H_2O$, Cement and Concrete Research 20 (1990) 941–947.
[81] S.J. Barnett, C.D. Adam, A.R.W. Jackson, An XRPD profile fitting investigation of the solid solution between ettringite, $Ca_6Al_2(SO_4)3(OH)_{12}{\times}26H_2O$, and carbonate ettringite, $Ca_6Al_2(CO_3)_3(OH)_{12}{\times}26H_2O$, Cement and Concrete Research 31 (2001) 13–17.
[82] T. Matschei, F.P. Glasser, New approaches to quantification of cement hydration. Proceedings of the 16th Ibausil, Weimar, 2006, Vol. I, 1-0389 - 1-0400.
[83] N.J. Crammond, The thaumasite form of sulfate attack in the UK, Cement and Concrete Composites 25 (2003) 809–818.
[84] J.H.P. Aarndt van, S. Viesser, Thaumasite formation: a cause of deterioration of portland cement and related substances in the presence of sulphates, Cement and Concrete Research 5 (1975) 225–232.
[85] S.M. Torres, C.A. Kirk, C.J. Lynsdale, R.N. Swamy, J.H. Sharp, Thaumasite–ettringite solid solutions in degraded mortars, Cement and Concrete Research 34 (2004) 225–232.
[86] H. Kollmann, G. Struebel, Ettringit–Thaumasit–Mischkristalle von Brenk (Eifel), Chemie der Erde 40 (1981) 110–120.
[87] W. Lukas, Betonzerstoerung durch SO3–Angriff unter Bildung von Thaumasit und Woodfordit, Cement and Concrete Research 5 (1975) 503–518.
[88] F. Bellmann, On the formation of thaumasite $CaSiO_3{\times}CaSO_4{\times}CaCO_3{\times}15H_2O$: Part II, Advances in Cement Research 16 (2004) 55–60.
[89] E.P. Flint, L.S. Wells, Study of the system $CaO–SiO_2–H_2O$ and of the reaction of water on the anhydrous calcium silicates, Journal of Research of the National Bureau of Standards, A, Physics and. Chemistry 12 (1934) 751–783.
[90] P.S. Roller, G. Ervine, The system calcium oxide–silica–water at 30 °C. The association of silicate ion in dilute alkaline solution, Journal of the Chemical Society 62 (1940) 461–471.
[91] H.F.W. Taylor, Hydrated Calcium Silicates, Part I: Compound formation at ordinary temperatures, Journal of the Chemical Society 726 (1950) 3682–3690 (notes).
[92] S.A. Greenberg, T.N. Chang, Investigations of the colloidal hydrated calcium silicates. II Solubility relationships in the calcium oxide-silica-water system at 25 °C, The Journal of Physical Chemistry 69 (1965) 182–188.
[93] K. Fuji, W. Kondo, Heterogeneous equilibrium of calcium silicate hydrate in water at 30 °C, Journal of the Chemical Society, Dalton Transactions (2) (1981) 645–651.
[94] K. Suzuki, T. Nishikawa, S. Ito, Formation and carbonation of C–S–H in water, Cement and Concrete Research 15 (1985) 213–224.
[95] Barbarulo, R., Comportment de materiaux cimentaires: actions des sulfates et de la temperature. PhD-Thesis, University of Laval, Canada, 2002.
[96] Walker, C., Characterisation and solubility behaviour of synthetic calcium-silicate hydrates. PhD-Thesis, University of Bristol, UK, 2003.
[97] K. Fuji, W. Kondo, Estimation of thermochemical data for Calcium Silicate Hydrate (C–S–H), Journal of the American Ceramic Society 66 (1983) C 220–C 221.
[98] F.P. Glasser, D.E. Macphee, E.E. Lachowski, Compositional model for calcium silicate hydrate (C–S–H) Gels, their solubilities, and free energies of formation, Journal of the American Ceramic Society 70 (1987) 481–485.
[99] E.M. Gartner, H.M. Jennings, Thermodynamics of calcium silicate hydrates and their Solutions, Journal of the American Ceramic Society 70 (1987) 743–749.
[100] U.R. Berner, Modelling the incongruent dissolution of hydrated cement minerals', Radiochimica Acta 44/45 (1988) 387–393.
[101] M. Kersten, Aqueous solubility diagrams for cementitious waste stabililzation systems. 1. The CSH solid-solution system, Environmental Science and Technology 30 (1996) 2286–2293.
[102] D. Kulik, personal communication 2007.
[103] R. Barbarulo, H. Peycelon, S. Prene, Experimental study and modelling of sulfate sorption on calcium silicate hydrates, Annales de Chimie Science des Matériaux 28 (2003) S5–S10 (Suppl.).
[104] L. Divet, R. Randrianbololona, Delayed ettringite formation: the effect of temperature and basicity on the interaction of sulphate and C–S–H phase, Cement and Concrete Research 28 (1998) 357–363.
[105] T. Matschei, R. Skapa, B. Lothenbach, F.P. Glasser, The distribution of sulfate in hydrated Portland cement paste, Proceedings of the 12th Intern. Congress on the Chemistry of Cements, Montreal, 2007.
[106] I.G. Richardson, G.W. Groves, The incorporation of minor and trace elements into calcium silicate hydrate (C–S–H) gel in hardened cement pastes, Cement and Concrete Research 23 (1993) 131–138.
[107] M. Atkins, F.P. Glasser, A. Kindness, Phase relations and solubility modeling in the $CaO–SiO_2–Al_2O_3–MgO–SO_3–H_2O$-system: for application to blended cements, Materials Research Society Symposium, Proceedings, vol. 212, 1991, pp. 387–394.
[108] E.P. Flint, H. McMurdie, L.S. Wells, Hydrothermal and X-ray studies of the garnet–hydrogarnet series and the relationship of the series to hydration products of Portland cement, Journal of Research of the National Bureau of Standards 26 (1941) 13–33.
[109] T. Matschei, F.P. Glasser, Zum Einfluss von Kalkstein auf die Zementhydratation, Zement-Kalk-Gips 12 (2006) 078–087.
[110] T. Matschei, F.P. Glasser, New approaches to quantification of cement hydration. Proceedings of the 16th Ibausil, Weimar, 2006, Vol. I, 1-0389 - 1-0400.
[111] T. Matschei, F.P. Glasser, Interactions between Portland cement and carbon dioxide, Proceedings of the 12th ICCC, Montreal, 2007.
[112] B. Albert, B. Guy, D. Damidot, Water chemical potential: a key parameter to determine the thermodynamic stability of some cement phases in concrete? Cement and Concrete Research 36 (2006) 783–790.